Vol. 34 (1983), No. 3

THE MOTION OF TEST PARTICLES IN BLACK-HOLE BACKGROUNDS WITH NON-ZERO COSMOLOGICAL CONSTANT

Z. Stuchlík

Department of Physics, College of Mines, 708 33 Ostrava-Poruba, Czechoslovakia

Received 10 February 1982

ДВИЖЕНИЕ ПРОБНЫХ ЧАСТИЦ В ПОЛЕ ЧЕРНЫХ ДЫР В СЛУЧАЕ КОСМОЛОГИЧЕСКОЙ ПОСТОЯННОЙ ОТЛИЧНОЙ ОТ НУЛЯ

Как следствие современных индикаций существования космологической постоянной отличной от нуля дискутируются некоторые аспекты влияния $\Lambda \neq 0$ на характер движения пробных частиц в поле черных дыр. Написаны уравнения движения электрически заряженных частиц, и магнитных монополей в самой общей дионной метрике Керра-Ньюмена-де Ситтера. Для пространства-времени Керра-де Ситтера при помощи метода „Китайских ящиков" детально исследовано широтное движение. В анализе радиального движения в пространстве-времени Шварцшильда-де Ситтера внимание обращено на существование и стабильность круговых орбит и на качества чисто радиальных траекторий. В заключение обсуждается возможность построения модели Вселенной Эйнштейна-Штрауса-де Ситтера (то есть модели конденсаций Шварцшильда-де Ситтера, вложенных во Вселенную Фридмана с $\Lambda \neq 0$).

Due to the present indications of the existence of a non-zero cosmological constant, some aspects of the influence of $\Lambda \neq 0$ on the character of test-particle motion in black-hole backgrounds are discussed. Equations of motion of electrically charged particles and magnetic monopoles are written in the most general Kerr-Newman-de Sitter dyon background. For the Kerr-de Sitter spacetime, the latitudinal motion is examined in detail by using the "Chinese boxes" technique. The radial motion in the Schwarzschild-de Sitter background is considered with attention devoted to the existence and stability of circular orbits and to the properties of purely radial trajectories. Finally, the possibility of constructing an Einstein-Strauss-de Sitter model of the Universe (i.e. a model of Schwarzschild-de Sitter condensations in the Friedman Universe with a non-zero Λ-term) is discussed.

1. Introduction

Recently two independent experimental groups have given evidence for the existence of the electromagnetic neutrino rest energy $m_{\nu_e}c^2 \approx 30$ eV (to be exact 14 eV $< m_{\nu_e}c^2 <$ 46 eV) – see Lyubimov et al. (1980), and Reines et al. (1970). With this non-zero rest energy relic neutrinos make the main contribution to the average matter density of the Universe; if the sum of rest energies of known types of neutrino (ν_e, ν_μ, ν_τ) is greater than 20 eV, our Universe turns out to be closed, and if the sum is greater than 60 eV, the age of our Universe would be less than 10^{10} years in contradiction to the age of the oldest stars, and a non-zero cosmological constant Λ must be introduced in order to eliminate this contradiction (Zel'dovich and Syunyaev, 1980). Thus in the light of recent experiments the possibility of a non-zero Λ should be taken seriously, moreover, this possibility is in agreement with recent ideology of theoretical physics as stated by Zeldovich and Syunyaev (1980): if something is not zero inevitably, then it is non-zero.

The simplest solution of the Einstein equations with a non-zero cosmological constant and vanishing energy-momentum tensor is de Sitter spacetime which can be written in the static form

$$(1) \qquad ds^2 = -(1 - \tfrac{1}{3}\Lambda r^2)\,dt^2 + (1 - \tfrac{1}{3}\Lambda r^2)^{-1}\,dr^2 + r^2(d\theta^2 + \sin^2\theta\,d\varphi^2)\,.$$

For $\Lambda = 0$ the line element (1) describes Minkowskian geometry in spherical coordinates.

For positive values of Λ (corresponding to repulsion) the metric (1) has an apparent singularity at $r_c = (\Lambda/3)^{-1/2}$, which determines event horizons (cosmological) of the observer who is located at the origin of coordinates – any timelike geodesics can be chosen as the origin. The de Sitter metric (1) can be "kruskalized" and a conformal (Penrose-Carter) diagram of the geodesically complete de Sitter spacetime can be constructed; both future and past infinities of spacetime are spacelike and, therefore, the past event horizon of the origin is the boundary of the region which cannot be influenced from the origin, while the future event horizon is the boundary of the region which cannot influence the origin (see Gibbons and Hawking, 1977). The de Sitter spacetime is

Bull. Astron. Inst. Czechosl. **34** (1983), 129–149.

a geodesically complete spacetime of constant curvature (positive if $\Lambda > 0$) with topology $R^1 \times S^3$ – see Hawking and Ellis (1973), where the geometry is also expressed in some other coordinate systems. (If not stated otherwise, we shall consider the repulsive Λ term.)

Cosmological models expanding forever with repulsive Λ approach de Sitter spacetime asymptotically at large times, when the cosmological fluid can be treated as test particles. The cosmological event horizon of an observer is then the boundary of regions from which light can never reach the observer due to rapid expansion of the spacetime.

For negative values of Λ (corresponding to attraction) the metric (1) is regular, and is sometimes called anti-de Sitter spacetime; – details can be found in Hawking and Ellis (1973).

The black-hole asymptotically flat solutions (determined by the Kerr-Newman metric) have been studied extensively in recent years, but also the black-hole asymptotical de Sitter solutions were found and discussed by Carter (1973) and further investigated by Gibbons and Hawking (1977).

The purpose of this paper is to discuss the properties of test-particle trajectories in asymptotical de Sitter black-hole backgrounds with both repulsive and attractive cosmological Λ term. In Sec. 2 equations of motion of electrically charged particles and magnetic monopoles in the most general Kerr-Newman-de Sitter dyon metric are given, in Sec. 3 the latitudinal motion of test particles in the Kerr-de Sitter spacetime is studied, while radial motion of test particles in the Schwarzschild-de Sitter spacetime is discussed in Sec. 4 with interest devoted to circular orbits and radial trajectories. Finally the possibility of constructing a model of the Einstein-Strauss-de Sitter Universe (i.e. a model of Schwarzschild condensations immersed in the Friedman Universe with the cosmological constant Λ present) is considered in Sec. 5.

2. Equations of Motion of Test Particles in the Kerr-Newman-de Sitter Dyon Spacetime

The black-hole solutions which are asymptotically de Sitter were found by Carter (1973). In coordinates of the Boyer-Lindquist type the Kerr-Newman-de Sitter dyon metric is described by the line element

$$(2)\qquad ds^2 = -\frac{\Delta_r}{I^2\varrho^2}(dt - a\sin^2\theta\, d\varphi)^2 + \frac{\Delta_\theta \sin^2\theta}{I^2\varrho^2}[a\, dt - (r^2 + a^2)\, d\varphi]^2 + \frac{\varrho^2}{\Delta_r}dr^2 + \frac{\varrho^2}{\Delta_\theta}d\theta^2 ,$$

where

$$(3a)\quad \varrho^2 = r^2 + a^2\cos^2\theta ,$$

$$(3b)\quad \Delta_r = (1 - \tfrac{1}{3}\Lambda r^2)(r^2 + a^2) - 2Mr + Q^2 + P^2 ,$$

$$(3c)\quad \Delta_\theta = 1 + \tfrac{1}{3}a^2\Lambda\cos^2\theta ,$$

$$(3d)\quad I = 1 + \tfrac{1}{3}a^2\Lambda .$$

The source has mass M, angular momentum per unit mass a, electric charge Q, and magnetic monopole charge P; geometrical units with $c = G = 1$ are used.

The electromagnetic field of the source is given by the vector potential

$$(4)\qquad A_\mu = \frac{1}{I\varrho^2}\{(Qr + aP\cos\theta)\,\delta^t_\mu - [aQr\sin^2\theta + (r^2 + a^2)P\cos\theta]\,\delta^\varphi_\mu\} .$$

The conformal (Penrose-Carter) diagram of the symmetry axis of the Kerr-Newman-de Sitter metric for the case that Δ_r has four zeros can be found in Gibbons and Hawking (1977) (or in Carter, 1973). The Kerr-Newman-de Sitter metric then has two black-hole horizons (an outer at r_+, an inner at r_-), and two cosmological horizons (one for positive radii at r_{++}, one for negative radii at r_{--}).

The motion of a test particle with rest mass m and electric charge e is determined by the Lorentz equation

$$(5)\qquad m\frac{Du^\mu}{D\tau} = eF^\mu_\nu u^\nu ,$$

where τ is the proper time of the particle, $u^\mu = dx^\mu/d\tau$ is its 4-velocity,and $F^\mu_\nu = A^\nu_{;\mu} - A^\mu_{;\nu}$ is the electromagnetic tensor of the background. The equations of motion (5) can be obtained from the Lagrangean

$$(6)\qquad \mathscr{L} = \tfrac{1}{2}g_{\mu\nu}\frac{dx^\mu}{d\lambda}\frac{dx^\nu}{d\lambda} - eA_\mu\frac{dx^\mu}{d\lambda}$$

where the affine parameter λ is related to the proper time of the particle by $\tau = m\lambda$. Thus the normalization condition is

$$(7)\qquad g_{\mu\nu}\frac{dx^\mu}{d\lambda}\frac{dx^\nu}{d\lambda} = -m^2 ;$$

the rest mass m is the first constant of motion. As both the line element (2) and the vector potential (4) are independent of coordinates t and φ, the corresponding momenta

$$(8)\qquad p_\varphi = \frac{\partial\mathscr{L}}{\partial(d\varphi/d\lambda)} = g_{\varphi\nu}\frac{dx^\nu}{d\lambda} - eA_\varphi = \Phi ,$$

$$(9)\qquad p_t = \frac{\partial \mathscr{L}}{\partial(\mathrm{d}t/\mathrm{d}\lambda)} = g_{tv}\frac{\mathrm{d}x^v}{\mathrm{d}\lambda} - eA_t = -E\,,$$

must be constants of the motion. Note, however, that E and Φ cannot be interpreted as energy and axial angular momenta at infinity due to the presence of the cosmological Λ term.

As in the case of the Kerr-Newman metric, a fourth constant of motion $\mathscr{K}$ can be obtained by using the Hamilton-Jacobi methods (see for example Misner et al., 1973) which enables us to give the equations of motion in a separated form:

$$(10)\qquad \varrho^2\frac{\mathrm{d}r}{\mathrm{d}\lambda} = \pm\,[R(r)]^{1/2}\,,$$

$$(11)\qquad \varrho^2\frac{\mathrm{d}\theta}{\mathrm{d}\lambda} = \pm\,[W(\theta)]^{1/2}\,,$$

$$(12)\qquad \varrho^2\frac{\mathrm{d}\varphi}{\mathrm{d}\lambda} = -\frac{IP_\theta}{\Delta_\theta \sin^2\theta} + \frac{aIP_r}{\Delta_r}\,,$$

$$(13)\qquad \varrho^2\frac{\mathrm{d}t}{\mathrm{d}\lambda} = -\frac{aIP_\theta}{\Delta_\theta} + \frac{(r^2+a^2)IP_r}{\Delta_r}\,,$$

where

$$(14)\qquad R = P_r^2 - \Delta_r(m^2r^2 + \mathscr{K})\,,$$

$$(15)\qquad W = (\mathscr{K} - a^2m^2\cos^2\theta)\Delta_\theta - \left(\frac{\mathsf{P}_\theta}{\sin\theta}\right)^2\,,$$

$$(16)\qquad \mathsf{P}_r = IE(r^2+a^2) - Ia\Phi - eQr\,,$$

$$(17)\qquad P_\theta = IaE\sin^2\theta - I\Phi + eP\cos\theta\,.$$

One can also easily find the equations of motion of the magnetic monopoles in the background (2). Due to the duality invariance, the motion of a particle with magnetic monopole charge $\mathbf{g}$ is given by the equation

$$(5')\qquad m\frac{\mathrm{D}u^\mu}{\mathrm{D}\tau} = \mathbf{g}{}^*F^\mu_\nu u^\nu\,.$$

Since the tensor ${}^*F^\mu_\nu$ which is dual to the tensor F^μ_ν is determined by the vector potential (4) where changes $Q \to P$, $P \to -Q$ are made, one can see immediately that trajectories of the magnetic monopoles are again given by equations (10)–(15), with

$$(18)\qquad \mathsf{P}_r = IE(r^2+a^2) - Ia\Phi - \mathbf{g}Pr\,,$$

$$(19)\qquad \mathsf{P}_\theta = IaE\sin^2\theta - I\Phi - \mathbf{g}Q\cos\theta\,.$$

Notice that the radial motion is influenced by interactions of electric (or magnetic) charges of the source and the particle, while the latitudinal motion is influenced by their mixed electro-magnetic interaction. Moreover, from (16)–(19) it is clear that motion of magnetic monopoles in the dyon metric (2) is of the same character as that of electric charges.

The equations (10)–(19) are valid for both positive and negative values of the cosmological parameter Λ; for $\Lambda = 0$ we obtain the Carter equations of motion of test particles in the Kerr-Newman metric (see, e.g., Misner et al., 1973). If $e = \mathbf{g} = 0$, Eqs (10)–(17) yield timelike geodesics, and if, moreover, $m = 0$ these equations determine null geodesics.

3. The Latitudinal Motion of Test Particles in the Kerr-de Sitter Spacetime

Because the latitudinal equation of motion (11) does not depend on the mass parameter M, the character of the latitudinal motion will be the same for both black-hole and naked-singularity spacetimes.

The latitudinal motion of neutral test particles in the Kerr metric was studied by de Felice and Calvani (1972), and by Bičák and Stuchlík (1976). The results of these papers hold equally for electrically charged particles in the Kerr-Newman metric with $P = 0$. The more general case of motion of electric charges or magnetic monopoles in the Kerr-Newman dyon metric was discussed quite recently by Calvani and Stuchlík (1982) – in this case the latitudinal motion is not symmetric with respect to the equatorial plane of the background.

The most general case with both magnetic monopole charge P and cosmological Λ term present in (15) and (17) is too complex and that is the reason why we will devote our attention only to the influence of the cosmological constant on the character of the latitudinal motion with $P = 0$.

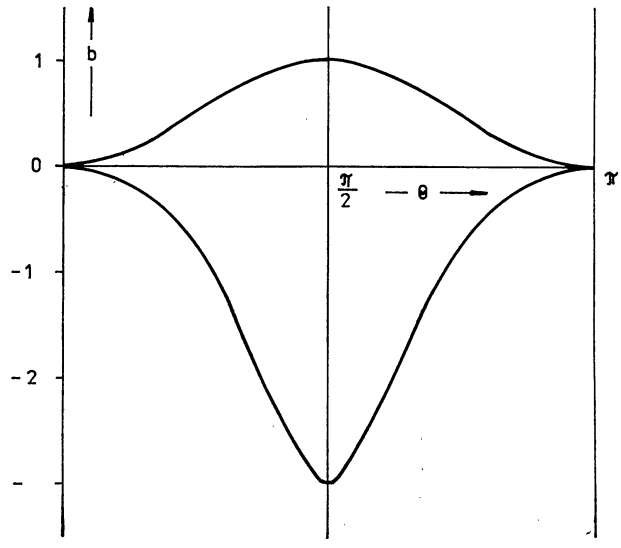

Fig. 1. Behaviour of the curves $\mathrm{b}^0_{e\pm}(\theta; y)$ in the case $0 < y < 1$. The curves are drawn for $y = 0{\cdot}5$.

Under the assumption $P = 0$ the expressions (15) and (17) become considerably simplified and Eq. (11) can be written as

$$(20)\quad \varrho^4 \left(\frac{d\theta}{d\lambda}\right)^2 = (\mathscr{K} - a^2m^2\cos^2\theta)\,\Delta_\theta - \frac{I^2(aE\sin^2\theta - \Phi)^2}{\sin^2\theta}.$$

In order to find the character of the latitudinal motion, the locus of turning points (solutions of eq. $d\theta/d\lambda = 0$) will be sought. From (20) it follows that the turning points are located on

$$(21)\quad \mathscr{K}_t = \frac{I^2(aE\sin^2\theta - \Phi)^2}{\Delta_\theta \sin^2\theta} + a^2m^2\cos^2\theta.$$

$\mathscr{K}_t(\theta; E, \Phi, a, m, \Lambda)$ represents a five-parameter family of curves in the $(\mathscr{K} - \theta)$ plane. Fortunately, by using the following rescalings and definitions

$$(22a)\quad \mathsf{K}_t = \frac{\mathscr{K}_t}{(aE)^2}, \quad \mathsf{b} = \frac{\Phi}{aE};$$

$$(22b)\quad \tilde{E} = E/m \quad y = \tfrac{1}{3}a^2\Lambda$$

we find that it is sufficient to consider only a three-parameter family of curves (for the case $E = 0$ see Appendix A)

$$(23)\quad \mathsf{K}_t(\theta; b, \tilde{E}, y) = \frac{(1+y)^2(\sin^2\theta - b)^2}{(1 + y\cos^2\theta)\sin^2\theta} + \frac{\cos^2\theta}{\tilde{E}^2}.$$

The behaviour of this family of curves can be studied most effectively by the "Chinese boxes" technique (see for example Calvani and Stuchlík, 1982). The physical dependence on the parameters can be clarified and illustrated in figures when this technique is used.

First, null geodesics ($m = 0$) will be discussed, and then we shall study the case of non-zero rest mass particles ($m \neq 0$); in both cases the discussion will be divided into four subcases in depending on the value of parameter y: $0 < y < 1$, $-1 < y < 0$, $y > 1$, $y < -1$. Recall however that only the first and the second subcases with $|y| \ll 1$ are of astrophysical interest, as in astrophysical situations the influence of the cosmological term can only be very small.

Note that from (23) it follows immediately, as in the case of the latitudinal motion of neutral particles in the Kerr metric, that the behaviour of the curves $\mathsf{K}_t = \mathsf{K}_t(\theta; \mathsf{b}, \tilde{E}, y)$ and of all their characteristics must always be symmetric with respect to the equatorial plane ($\theta = \frac{1}{2}\pi$) of the background. Therefore,

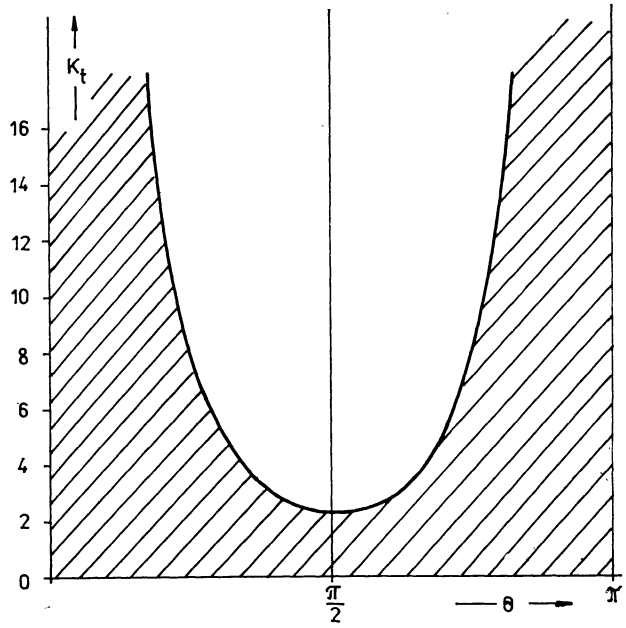

Fig. 2. Constant b-value section of the surface $\mathsf{K}_t = \mathsf{K}_t(\theta; \tilde{E}, \mathsf{b}, y)$ in the case when $\theta = \text{const}$ trajectories are possible only at $\theta = \frac{1}{2}\pi$, and are stable. The section is drawn for $m = 0$, $y = 0{\cdot}5$, $\mathsf{b} = 2$. The latitudinal motion is allowed along horizontal lines ($\mathsf{K} = \text{const}$) in the unshaded region and minima of K_t-sections determine stable $\theta = \text{const}$ trajectories, while maxima of K_t-sections give unstable $\theta = \text{const}$ orbits for all figures of the K_t-sections.

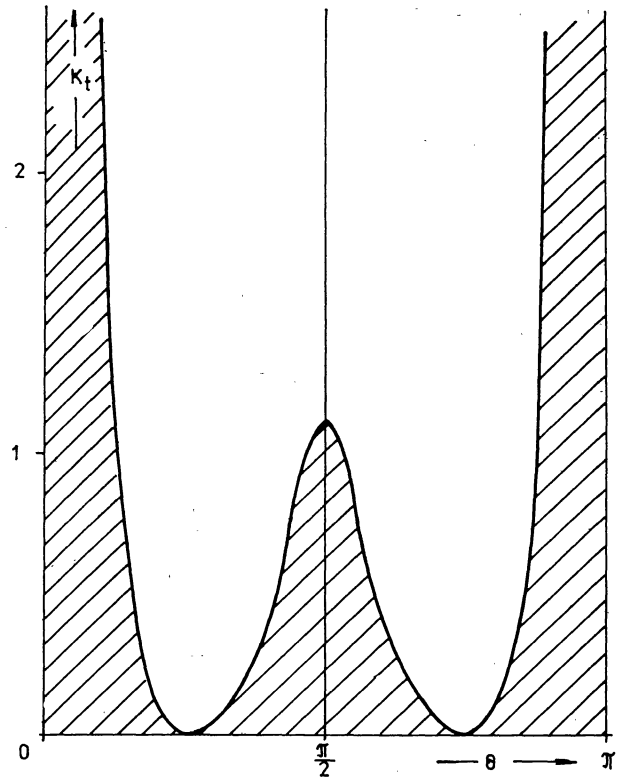

Fig. 3. K_t-section in the case when PNC photons on stable $\theta = \text{const}$ geodesics are given by the minima of K_t with $\mathsf{K}_{t\min} = 0$. The $\theta = \text{const}$ orbit must then always be unstable. The section is drawn for $m = 0$, $y = 0{\cdot}5$, $\mathsf{b} = 0{\cdot}5$.

it is sufficient to consider only $\theta \in \langle 0, \frac{1}{2}\pi\rangle$ in the discussion.

If $y > -1$ we can further say that $K_t(0) \to +\infty$ for $b \neq 0$, and $K_t(0) = \tilde{E}^{-2}$ for $b = 0$; the curves $K_t(\theta; b, \tilde{E}, y)$ are always positive-valued, and from (20) it is clear that only values of $K \geqq K_t(\theta; b, \tilde{E}, y)$ are allowed. Thus for $y > -1$ only positive values of the parameter K are possible.

On the other hand, if $y < -1$, the situation becomes more complex, because Δ_θ-term has zero at

$$\theta_e = \arccos(-y)^{-1/2}. \tag{24}$$

Thus for $y < -1$ the line element (2) is degenerate at θ_e. In this case the metric (2) has signature $+2$ at $\theta > \theta_e$, while at $\theta < \theta_e$ the signature changes into -2. Although Carter (1973) has imposed the restriction $1 + y > 0$ for the Kerr-de Sitter spacetime we also include here the case $y < -1$ in order to understand its character. The regions $\theta > \theta_e$ and $\theta < \theta_e$ can be considered as two spacetimes disconnected by the surface of degeneracy $\theta = \theta_e$, but in the $\theta < \theta_e$-region Eq. (23) determines spacelike geodesics, i.e. trajectories of tachyons with $m \neq 0$ being the meta-mass of the tachyons (see Appendix B).

Thus $K_t(0) \to -\infty$ for $b \neq 0$, and $K_t(0) = \tilde{E}^{-2}$ for $b = 0$; if $b \neq (y + 1)/y$ we have $\lim_{\theta \to \theta_e -} K_t = -\infty$, $\lim_{\theta \to \theta_e +} K_t \to +\infty$ while for $b = (y + 1)/y$ it is $K_t(\theta = \theta_e) = -(y\tilde{E}^2)^{-1} \geqq 0$. From (20) it follows that for $\theta \in \langle 0, \theta_e)$ values of $K \leqq K_t$ are allowed, while for $\theta \in (\theta_e, \frac{1}{2}\pi\rangle$ we obtain inequality $K \geqq K_t$. Consequently, if $y < -1$ negative values of K are possible at $\theta < \theta_e$.

After these general remarks a detailed discussion can be begun in which characteristic sections of constant values of the parameter b (and $\tilde{E}$, y) of the surface $K_t = K_t(\theta; b, \tilde{E}, y)$ will finally be drawn.

a) Zero-Rest-Mass Particles

Assuming $m = 0$ we arrive at the two-parameter family of curves

$$K_t(\theta; b, y) = \frac{(1 + y)^2 (\sin^2\theta - b)^2}{(1 + y\cos^2\theta)\sin^2\theta}. \tag{25}$$

The loci of the extrema of $K_t(\theta; b, y)$ are at $\theta = \frac{1}{2}\pi$, and in the $(b - \theta)$ plane they are described by functions

$$b^0_{e+}(\theta; y) = \sin^2\theta, \tag{26}$$

$$b^0_{e-}(\theta; y) = -\frac{(1 + y)\sin^2\theta}{1 + y\cos 2\theta}. \tag{27}$$

(Notice that b^0_{e+} does not depend on y.) One can show that the extreme points of curves $b^0_{e\pm}(\theta; y)$ are at $\theta = \frac{1}{2}\pi$, where $b^0_{e+}(\frac{1}{2}\pi, y) = 1$ (a maximum), $b^0_{e-}(\frac{1}{2}\pi; y) = (y + 1)/(y - 1)$ (a minimum). The common point of b^0_{e+} and b^0_{e-} is at $\theta = 0$, where $b^0_{e+} = b^0_{e-} = 0$.

i) $0 < y < 1$

The behaviour of curves $b^0_{e\pm}(\theta; y)$ is illustrated in Fig. 1; the inequality $b^0_{e-}(\frac{1}{2}\pi; y) < -1$ holds. For $b > 1$ or $b < (y + 1)/(y - 1)$ the characteristic sections of $K_t(\theta; b, y)$ are given in Fig. 2, for $0 < b < 1$ the sections of $K_t(\theta; b, y)$ are of the type shown in Fig. 3, and for $(y + 1)/(y - 1) < b < 0$ the sections are determined by Fig. 4. If $b = 0$, then

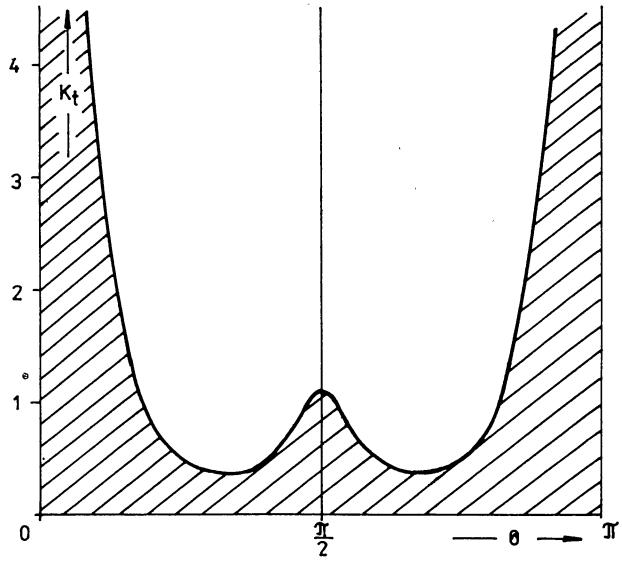

Fig. 4. K_t-section drawn for $y = 0{\cdot}5$, $\tilde{E}^2 = 1$, $b = 0{\cdot}5$, when $\theta =$ const trajectories are possible at $\theta \neq \frac{1}{2}\pi$, but $K_{tmin} > 0$.

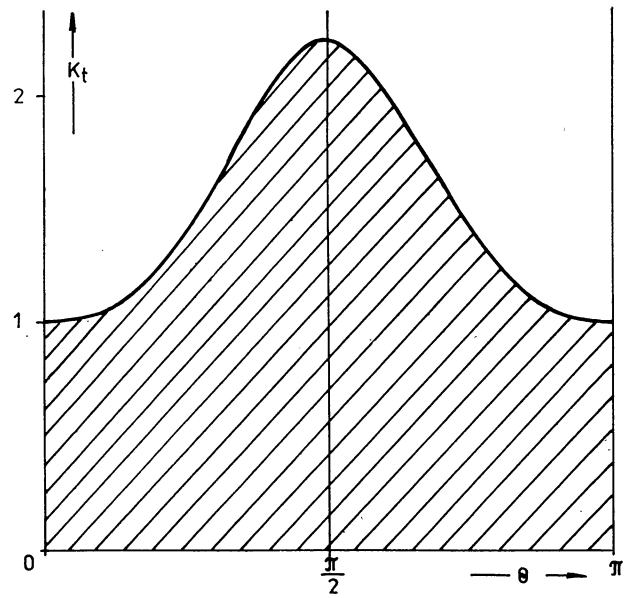

Fig. 5. K_t-section in the special case $b = 0$, drawn for $y = 0{\cdot}5$, $\tilde{E}^2 = 1$.

for all $y > -1$ the characteristic sections of $K_t(\theta; b = 0, y)$ are the same as those of Fig. 5, but $K_t(\theta = 0) = 0$.

It should be noted that for all values of y the extreme points of $K_t(\theta; b, y)$ determined by the curve b^0_{e+} have $K_{t,extr} = 0$. The photons corresponding to these extreme points move with constant but arbitrary latitudes θ along null geodesics which are stable with respect to perturbations in the θ-direction. The family of these geodesics is called the principal null congruence (PNC) and is privileged by the spacetime geometry (see Carter, 1973; Misner et al., 1973). Thus we can conclude that in Kerr-Newman-de Sitter spacetime the PNC photons must have $K = 0$, in agreement with results obtained in the Kerr spacetime (Bičák and Stuchlík, 1976).

ii) $-1 < y < 0$

The curves $b^0_{e\pm}(\theta, y)$ are again smooth, but the inequality $-1 < b^0_{e-}(\frac{1}{2}\pi) < 0$ must hold (see Fig. 6). The characteristic sections of the surface K_t are given in the same manner as for $0 < y < 1$.

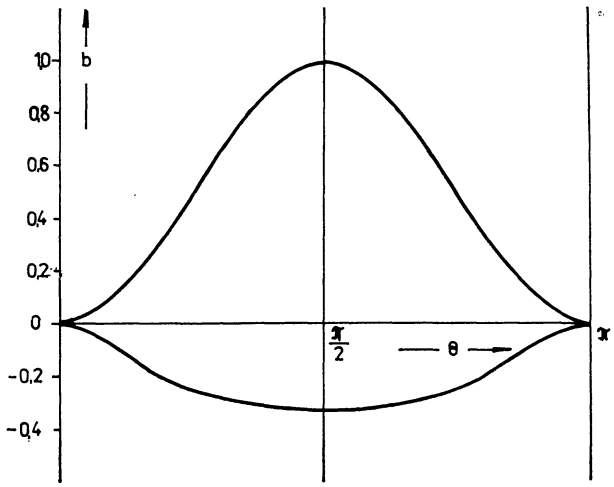

Fig. 6. Behaviour of the curves $b^0_{e\pm}(\theta; y)$ in the case $-1 < y < 0$. The figure is plotted for $y = -0{\cdot}5$.

iii) $y > 1$

In this case the curve $b^0_{e-}(\theta; y)$ is discontinous at

$$\theta_r = \tfrac{1}{2}\arccos(-y)^{-1}, \tag{28}$$

where $\lim_{\theta\to\theta_{r-}} b^0_{e-} = -\infty$, $\lim_{\theta\to\theta_{r+}} b^0_{e+} = +\infty$; further $b^0_{e-}(\frac{1}{2}\pi) > 1$ (see Fig. 7). The behaviour of sections of $K_t(\theta; b, y)$ has the following character: for $b < 0$ and $b > (y+1)/(y-1)$ it is given by Fig. 4, for $0 < b < 1$ Fig. 3 is relevant, and for $1 < b < (y+1)/(y-1)$ it is determined by Fig. 2.

iv) $y < -1$

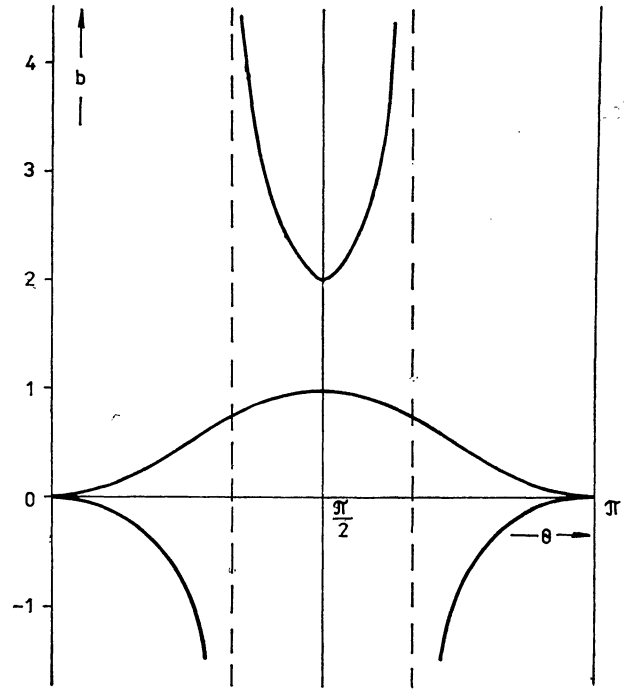

Fig. 7. Behaviour of the curves $b^0_{e\pm}(\theta; y)$ in the case $y > 1$ (drawn for $y = 2$).

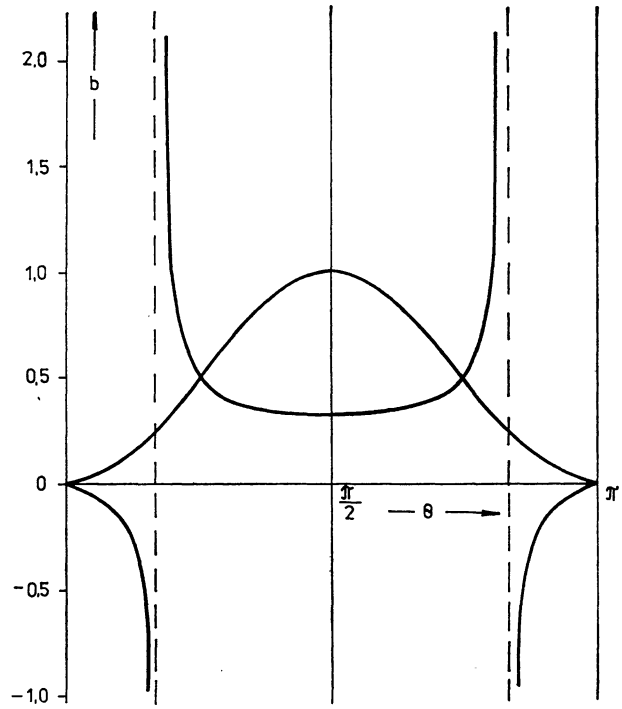

Fig. 8. Behaviour of the curves $b^0_{e\pm}(\theta; y)$ in the case $y < -1$. The curves are plotted for $y = -2$.

Now the curve $b^0_{e-}(\theta; y)$ is again discontinuous at θ_r, as given by (28), but $0 < b^0_{e-}(\frac{1}{2}\pi) < 1$. The curves b^0_{e+} and b^0_{e-} have point of intersection at $\theta = \theta_e$,

as given by (26) ($\theta_r < \theta_e$), where $\mathsf{b}^0_{e+}(\theta_e) = \mathsf{b}^0_{e-}(\theta_e) = (y+1)/y$, see Fig. 8. Thus for $\mathsf{b} < 0$ or $\mathsf{b} > 1$ the section of K_t is demonstrated in Fig. 9, while for $(y+1)/y < b < 1$ the section is shown in Fig. 10, which is relevant also for $(y+1)/(y-1) < \mathsf{b} < (y+1)/y$, but in this case there is $\mathsf{K}_t = 0$ in the maximum at $\theta < \theta_e$. Fig. 9 can also be used if $0 < \mathsf{b} < (y+1)/(y-1)$, but again there is $\mathsf{K}_t = 0$ in the maximum at $\theta < \theta_e$. In the special case $\mathsf{b} = (y+1)/y$ the section of $\mathsf{K}_t(\theta; \mathsf{b}, y)$ is given by Fig. 11, while for $\mathsf{b} = 0$ its behaviour is determined by Fig. 12 with $\mathsf{K}_t(\theta = 0) = 0$.

b) *Non-Zero-Rest-Mass Particles*

The extrema of the surface $\mathsf{K}_t(\theta; \mathsf{b}, \tilde{E}, y)$ as given by (23) are located on the curves

$$\mathsf{b}_{e\pm}(\theta; \tilde{E}, y) = \frac{(-y \sin^2\theta \pm \Delta_\theta A)\sin^2\theta}{1 + y\cos 2\theta}, \tag{29}$$

where

$$A = \left[1 - \frac{1 + y\cos 2\theta}{(1+y)^2 \tilde{E}^2}\right]^{1/2}, \tag{30}$$

and at $\theta = \frac{1}{2}\pi$.

Now the behaviour of the curves $\mathsf{b}_{e\pm}(\theta; \tilde{E}, y)$ will be determined. The reality condition on $b_{e\pm}(\theta; \tilde{E}, y)$ (and namely on A) is

$$\tilde{E}^2 \geqq \tilde{E}^2_r(\theta, y), \tag{31}$$

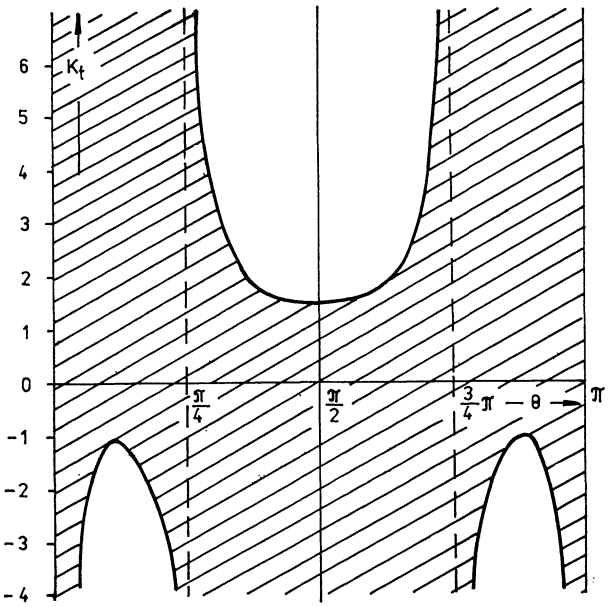

Fig. 9. K_t-section plotted for $m = 0$, $y = -2$, $\mathsf{b} = -0{\cdot}2$. For $y < -1$ orbits with negative values of the parameter K are possible at $\theta \in (0, \theta_e)$.

where

$$\tilde{E}^2_r(\theta; y) = \frac{1 + y\cos 2\theta}{(1+y)^2}. \tag{32}$$

The marginal value of $\theta \neq 0$, where $\mathsf{b}_{e+} = \mathsf{b}_{e-}$, is given by

$$\theta_m = \frac{1}{2}\arccos\left[\frac{(1+y)^2\tilde{E}^2 - 1}{y}\right]. \tag{33}$$

For zeros of curves $\mathsf{b}_{e\pm}(\theta; \tilde{E}, y)$ we obtain

$$\tilde{E}^2_z(\theta; y) = \frac{(1 + y\cos^2\theta)^2}{(1+y)^3}. \tag{34}$$

The extrema of curves $\mathsf{b}_{e\pm}(\theta; \tilde{E}, y)$ are at $\theta = \frac{1}{2}\pi$ (if the curves are defined here) and on curves

$$\tilde{E}^2_{e\pm}(\theta; y) = \frac{1}{(1+y)^4} \cdot \tag{35}$$

$$\cdot \{(1 + y\cos 2\theta)[(1+y)^2 - y\Delta_\theta \sin^2\theta] \pm$$

$$\pm 2y\Delta_\theta \sin^3\theta[-y\Delta_\theta]^{1/2}\}.$$

Therefore at $\theta \neq \frac{1}{2}\pi$ the extrema of $\mathsf{b}_{e\pm}(\theta; \tilde{E}, y)$ can exist only for $y < 0$.

One can easily show that the curves $\tilde{E}^2_r(\theta; y)$,

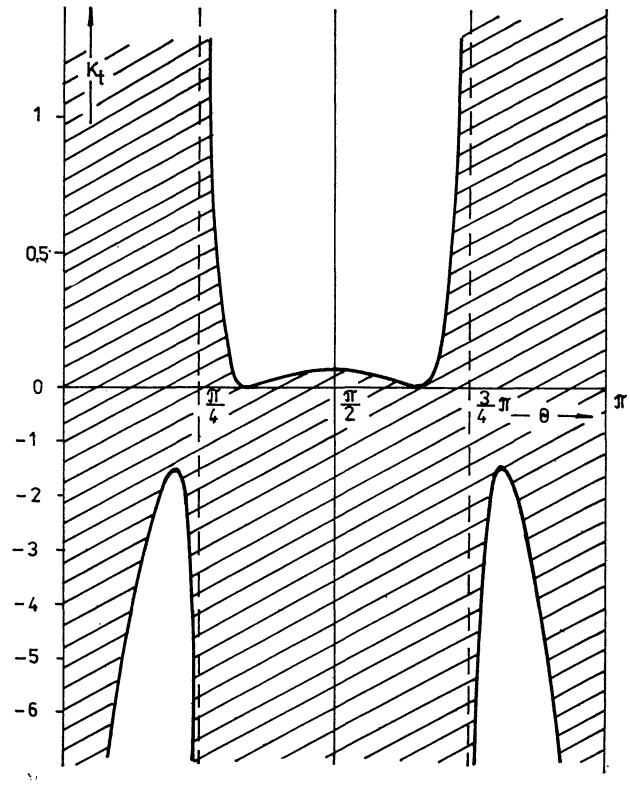

Fig. 10. K_t-section in the case $m = 0$, $y = -2$, $\mathsf{b} = 0{\cdot}75$. The minima here again determine the PNC photons.

$\tilde{E}_z^2(\theta; y)$, $\tilde{E}_{e\pm}^2(\theta; y)$ have only one extreme point at $\theta = \frac{1}{2}\pi$, where

$$(36)\quad \tilde{E}_r^2(\tfrac{1}{2}\pi) = \frac{1-y}{(1+y)^2}, \quad \tilde{E}_z^2(\tfrac{1}{2}\pi) = \frac{1}{(1+y)^3},$$

$$\tilde{E}_{e\pm}^2(\tfrac{1}{2}\pi) = \frac{1}{(1+y)^4}\left[1 - y^3 \pm 2y(-y)^{1/2}\right].$$

Further, for all values of y we have

$$(37a)\qquad \tilde{E}_r^2(0) = \tilde{E}_z^2(0) = \frac{1}{1+y},$$

and for $y > -1$ it is also

$$(37b)\qquad \tilde{E}_{e\pm}^2(0) = \frac{1}{1+y}.$$

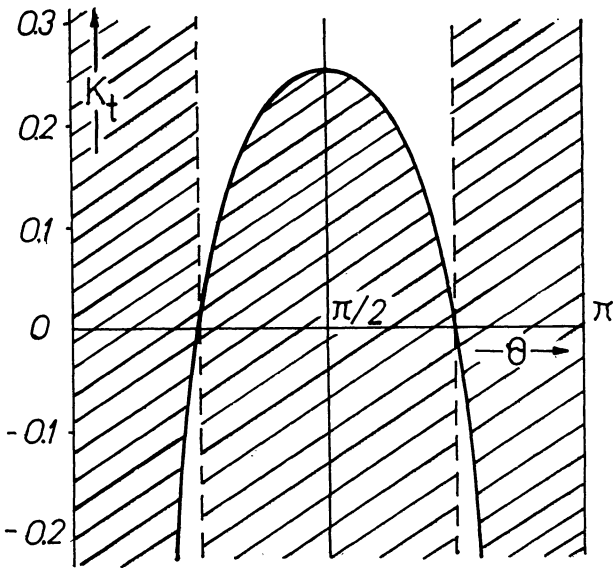

Fig. 11. K_t-section which characterizes the special case $b = (y+1)/y$ for $y < -1$. The figure is drawn for $m = 0$, $y = -2$, $b = 0{\cdot}5$.

(Of course, the curves $\tilde{E}_r^2(\theta; y)$, $\tilde{E}_z^2(\theta; y)$, $\tilde{E}_{e\pm}^2(\theta, y)$ are defined only if $\tilde{E}^2 \geqq 0$.)

In the special case of $b = 0$, the expression (23) is reduced to

$$(38)\quad K_t(\theta; \tilde{E}, y) = \frac{(1+y)^2 \sin^2\theta}{1 + y\cos^2\theta} + \frac{\cos^2\theta}{\tilde{E}^2},$$

the extrema of which are located on the curve $\tilde{E}_z^2(\theta, y)$, given by (34), and at $\theta = \frac{1}{2}\pi$. If $y > -1$, the curves $K_t(\theta; \tilde{E}, y)$ have a maximum at $\theta = \frac{1}{2}\pi$ for $\tilde{E}^2 > (1+y)^{-3}$, and a minimum for $\tilde{E}^2 < (1+y)^{-3}$. If $y < -1$, then curves $K_t(\theta; \tilde{E}, y)$ have a minimum at $\theta = \frac{1}{2}\pi$ for all $\tilde{E}^2 \geqq 0$.

i) $0 < y < 1$

The curves $\tilde{E}_r^2(\theta; y)$ and $\tilde{E}_z^2(\theta; y)$ are defined and continuous for all θ; they have no point of intersection, and from (36) and (37) it follows that $\tilde{E}_r^2(\frac{1}{2}\pi) < \tilde{E}_z^2(\frac{1}{2}\pi) < \tilde{E}_r^2(0)$ – see Fig. 13. Now the behaviour of $b_{e\pm}(\theta; \tilde{E}, y)$ can be determined: for $\tilde{E}^2 > (1+y)^{-1}$ (see Fig. 14a) the curves are defined for all values of θ, while for $(1+y)^{-1} > \tilde{E}^2 > (1+y)^{-3}$ (see Fig. 14b), where positive values of b_{e+} are allowed, and for $(1+y)^{-3} > \tilde{E}^2 > (1-y)/(1+y)^2$ (see Fig. 14c), where all values of curves $b_{e\pm}$ must be negative, the curves are defined for $\theta \in \langle\theta_m, \frac{1}{2}\pi\rangle$, with θ_m given by (33). For $\tilde{E}^2 < (1-y)/(1+y)^2$ curves $b_{e\pm}$ are not defined.

The character of sections of the surface $K_t(\theta; b, \tilde{E}, y)$ can be found in the following manner: if a line $b =$ $=$ const $\neq 0$ intersects curves $b_{e\pm}$, then the characteristic section of $K_t(\theta; b, \tilde{E}, y)$ is determined by Fig. 4 (stable $\theta =$ const $\neq \frac{1}{2}\pi$ orbits, and orbits of the vortical type can exist, but the equatorial orbits are unstable), while if the $b =$ const $\neq 0$ line does not intersect curves $b_{e\pm}$ (or if these curves are not defined), the behaviour of sections of $K_t(\theta; b, \tilde{E}, y)$ is demonstrated in Fig. 2 (no vortical motion, but the equatorial trajectories are stable). Thus we can conclude that the vortical motion is only possible for $\tilde{E}^2 > (1-y)/(1+y)^2$ if $b \in \langle b_{e-}(\frac{1}{2}\pi), b_{e+}(\frac{1}{2}\pi)\rangle$, where

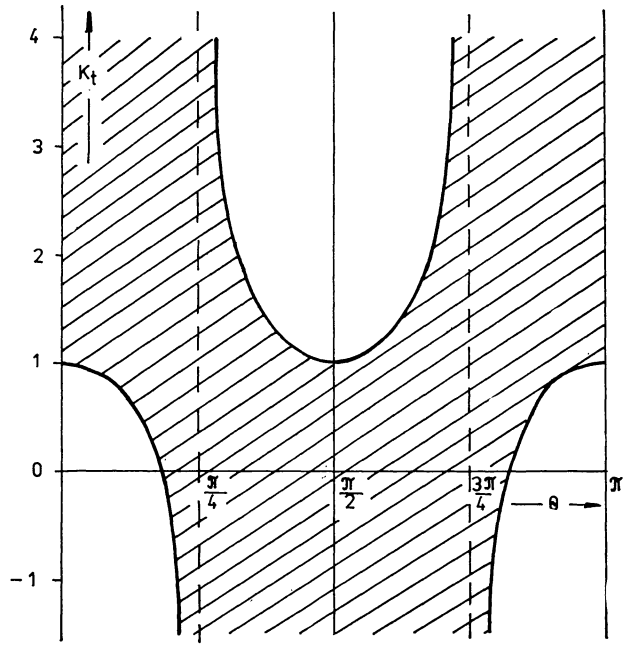

Fig. 12. K_t-section in the special case $b = 0$. The section is plotted for $y = -2$, $\tilde{E}^2 = 1$.

$$(39)\quad b_{e\pm}(\tfrac{1}{2}\pi) = \frac{1}{1-y}\left\{-y \pm \left[1 - \frac{1-y}{(1+y)^2\tilde{E}^2}\right]^{1/2}\right\},$$

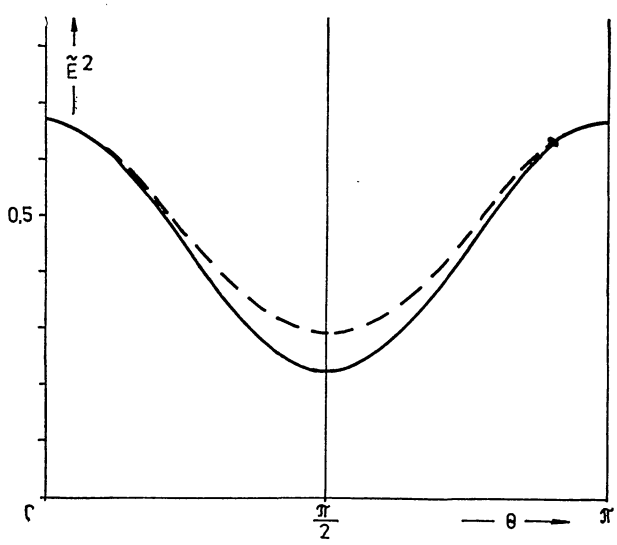

Fig. 13. Behaviour of the curves $\tilde{E}_r^2(\theta; y)$ (solid curve), $\tilde{E}_z^2(\theta; y)$ (dashed curve) for $0 < y < 1$; the curves are plotted for $y = 0{\cdot}5$.

If $y < -0{\cdot}2956$, the inequality

$$\tilde{E}_{e-}^2(\tfrac{1}{2}\pi) > \tilde{E}_z^2(\tfrac{1}{2}\pi) > \tilde{E}_{e+}^2(\tfrac{1}{2}\pi) > \tilde{E}_r^2(\tfrac{1}{2}\pi) > \tilde{E}_r^2(0) \tag{40}$$

holds (see Fig. 17). There is an intersection point of curves $\tilde{E}_z^2(\theta; y)$ and $\tilde{E}_{e+}^2(\theta, y)$ at

$$\theta_i = \arcsin\left[-\frac{1+y}{3y}\left(2\cosh\frac{\eta}{3} - 1\right)\right]^{1/2},$$

where $\cosh\eta = \frac{19}{8}$.

Thus we have six different possibilities for curves $\mathsf{b}_{e\pm}(\theta; \tilde{E}, y)$ which correspond to six ranges of parameter $\tilde{E}^2$ (see Fig. 18):

a) $\tilde{E}^2 > \tilde{E}_{e-}^2(\tfrac{1}{2}\pi)$,

b) $\tilde{E}_{e-}^2(\tfrac{1}{2}\pi) > \tilde{E}^2 > \tilde{E}_z^2(\tfrac{1}{2}\pi($,

c) $\tilde{E}_z^2(\tfrac{1}{2}\pi) > \tilde{E}^2 > \tilde{E}_{e+}^2(\tfrac{1}{2}\pi)$,

d) $\tilde{E}_{e+}^2(\tfrac{1}{2}\pi) > \tilde{E}^2 > \tilde{E}_r^2(\tfrac{1}{2}\pi)$,

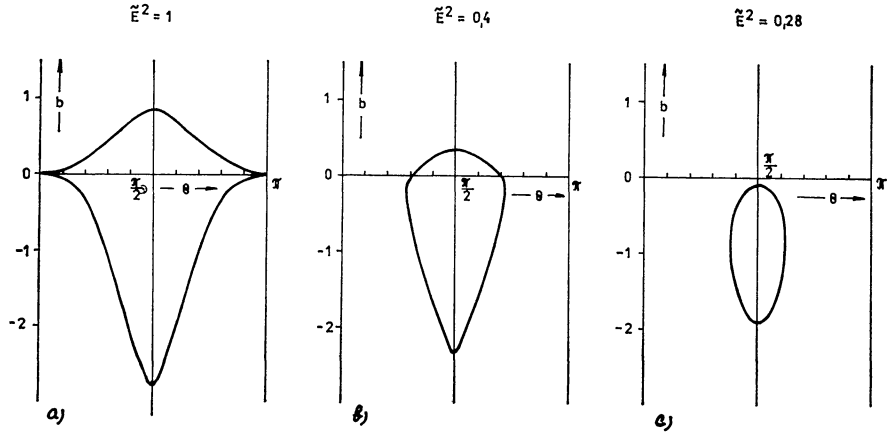

Fig. 14. Sequence of figures giving typical behaviour of the curves $\mathsf{b}_{e\pm}(\theta; \tilde{E}^2, y)$ in the $0 < y < 1$ case. The figures are drawn for $y = 0{\cdot}5$. The sequence is labelled by values of $\tilde{E}^2$ for which the figures are plotted.

and the stable $\theta = \text{const} \neq \frac{1}{2}\pi$ orbits can exist at any θ for $\tilde{E}^2 > 1/(1+y)$ only. If $\tilde{E}^2 < (1+y)^{-1}$, these orbits can exist at $\theta \in \langle\theta_m, \frac{1}{2}\pi)$. For $(1+y)^{-3} > \tilde{E}^2 > (1-y)/(1+y)^2$ motion of the vortical type is only possible for negative values of b. The vortical motion is allowed for $\mathsf{K} \in \langle \mathsf{K}_{t\min}, \mathsf{K}_t(\frac{1}{2}\pi)\rangle$, where $\mathsf{K}_{t\min}$ is value of the curve $\mathsf{K}_t(\theta; \mathsf{b}, \tilde{E}, y)$ at its minimum, and $\mathsf{K}_t(\frac{1}{2}\pi) = (1+y)^2(1-\mathsf{b})^2$.

For $\mathsf{b} = 0$ the behaviour of the characteristic sections of K_t is shown in Fig. 5 [for $E^2 > (1+y)^{-1}$] in Fig. 15 [for $(1+y)^{-1} > \tilde{E}^2 > (1+y)^{-3}$; the vortical motion is possible], and in Fig. 16 [for $\tilde{E}^2 < (1+y)^{-3}$].

ii) $-1 < y < 0$

In this case all curves $\tilde{E}_r^2(\theta; y)$, $\tilde{E}_z^2(\theta; y)$, $\tilde{E}_{e\pm}^2(\theta; y)$ are defined and continuous for all values of θ.

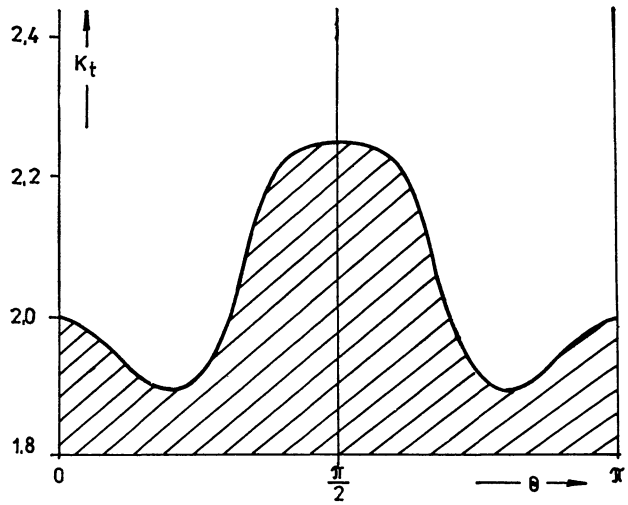

Fig. 15. K_t-section in the special case $\mathsf{b} = 0$ for $y = 0{\cdot}5$, $\tilde{E}^2 = 0{\cdot}5$.

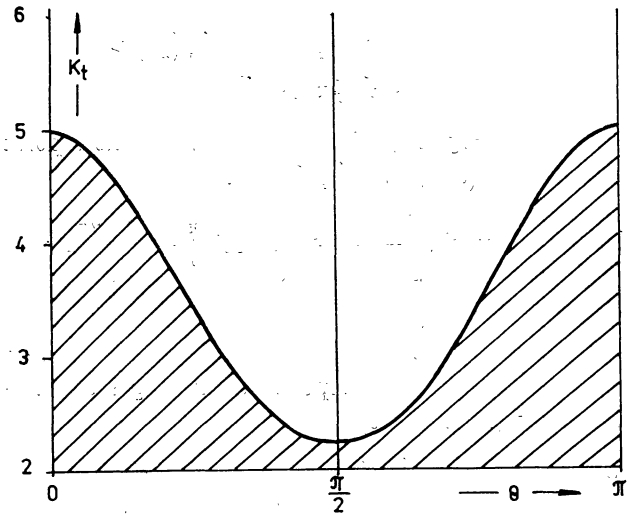

Fig. 16. K_t-section drawn in the special case $b = 0$ for $y = 0{\cdot}5$, $\tilde{E}^2 = 0{\cdot}2$.

e) $\tilde{E}_r^2(\frac{1}{2}\pi) > \tilde{E}^2 > \tilde{E}_r^2(0)$,

f) $\tilde{E}^2 < \tilde{E}_r^2(0)$ – curves $b_{e\pm}(\theta; \tilde{E}, y)$

are not defined.

If $y > -0{\cdot}2956$, inequality (40) is valid with one exception: $\tilde{E}_{e+}^2(\frac{1}{2}\pi) > \tilde{E}_z^2(\frac{1}{2}\pi)$; therefore, there is no point of intersection of curves $\tilde{E}_z^2(\theta; y)$; $\tilde{E}_{e\pm}^2(\theta; y)$ in Fig. 17. Thus Fig. 18c disappears from the sequence

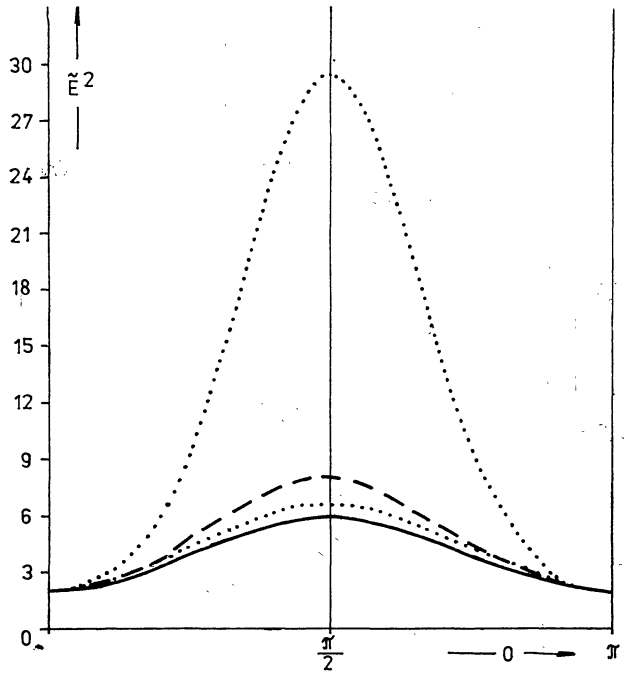

Fig. 17. Behaviour of the curves $\tilde{E}_r^2(\theta; y)$ (solid curve), $\tilde{E}_z^2(\theta; y)$ (dashed curve), $\tilde{E}_{e\pm}^2(\theta; y)$ (dotted curves) in the $-1 < y < 0$ case. The curves are drawn for $y = -0{\cdot}5$ and therefore curves $\tilde{E}_z^2$ and $\tilde{E}_{e+}^2$ must intersect each other at $\theta = \theta_i$.

of Figs 18a–e, and for $\tilde{E}_{e+}^2(\frac{1}{2}\pi) > \tilde{E}^2 > \tilde{E}_z^2(\frac{1}{2}\pi)$ the behaviour of $b_{e\pm}(\theta; \tilde{E}, y)$ is shown in Fig. 19. The rest of the sequence of Figs 18 is still relevant, but the lower boundary in range b) and the upper boundary in range d) must be replaced.

If there is one intersection of a line $b = \text{const} \neq 0$ with the curves $b_{e\pm}(\theta; \tilde{E}, y)$ at $\theta \in (0, \frac{1}{2}\pi)$ (we shall θ always be referring to this interval below), the character of $b = \text{const}$ sections of $K_t(\theta; b, \tilde{E}, y)$ is determined by Fig. 4, while for two points of intersection of $b = \text{const} \neq 0$ line with $b_{e\pm}(\theta; \tilde{E}, y)$ Fig. 20 characterizes the section of $K_t(\theta; b, \tilde{E}, y)$ – the first point gives a minimum $K_{t\min}$ of the section (with a stable $\theta = \text{const}$ trajectory), the second point gives a maximum $K_{t\max} > K_t(\frac{1}{2}\pi)$ of the section (with an unstable $\theta = \text{const}$ trajectory); vortical motion is then allowed for $K \in \langle K_{t\min}, K_{t\max}\rangle$. From Figs 18 and 19 it follows that for $(1 + y)^{-4}[1 - y^3 - 2y(-y)^{1/2}] > \tilde{E}^2 > (1 + y)^{-1}$ there always exist a range of parameter b which gives two extrema of $K_t(\theta; b, \tilde{E}, y)$. If the $b = \text{const} \neq 0$ line does not intersect curves $b_{e\pm}(\theta; \tilde{E}, y)$, the characteristic K_t-sections are demonstrated in Fig. 2.

For $b = 0$ the behaviour of sections of $K_t(\theta; b, \tilde{E}, y)$ is illustraten in Fig. 5 [for $\tilde{E}^2 > (1 + y)^{-3}$], in Fig. 16 [for $E^2 < (1 + y)^{-1}$], and in Fig. 21 [for $(1 + y)^{-3} > \tilde{E}^2 > (1 + y)^{-1}$].

iii) $y > 1$

Curve $\tilde{E}_z^2(\theta; y)$ is defined for $\theta \in \langle 0, \frac{1}{2}\pi\rangle$, while curve $\tilde{E}_r^2(\theta; y)$ is defined at $\theta \in \langle \theta_r, \frac{1}{2}\pi\rangle$, where θ_r is given by (28) – see Fig. 22. At θ_r the curve $b_{e-}(\theta; \tilde{E}, y)$ is discontinuous; it is $\lim_{\theta \to \theta_r -} b_{e-} = -\infty$, and $\lim_{\theta \to \theta_r +} b_{e-} = +\infty$; the curve b_{e+} is continuous at θ_r – see Fig. 23. There are three different possibilities for $b_{e\pm}(\theta; \tilde{E}, y)$ corresponding to three ranges of parameter $\tilde{E}^2$ (Fig. 23):

a) $\tilde{E}^2 > \tilde{E}_r^2(0)$,

b) $\tilde{E}_r^2(0) > \tilde{E}^2 > \tilde{E}_z^2(\frac{1}{2}\pi)$,

c) $\tilde{E}_z^2(\frac{1}{2}\pi) > \tilde{E}^2 > 0$.

Thus we can say that for any value of $\tilde{E}^2 > 0$ sections of $K_t(\theta; b, \tilde{E}, y)$ are given by Fig. 4 if $b > b_{e-}(\frac{1}{2}\pi)$ or $b < b_{e+}(\frac{1}{2}\pi)$, and are determined by Fig. 2 if $b_{e+}(\frac{1}{2}\pi) < b < b_{e-}(\frac{1}{2}\pi)$, where $b_{e\pm}(\frac{1}{2}\pi)$ are defined by (39); vortical motion is possible for any value of $\tilde{E}^2 > 0$. For $b = 0$ the behaviour of sections of $K_t(\theta; b, \tilde{E}, y)$ is the same as in the case $0 < y < 1$.

iv) $y < -1$

Curve $\tilde{E}_z^2(\theta; y)$ is not defined, curve $\tilde{E}_r^2(\theta; y)$ is defined for $\theta \in \langle \theta_r, \frac{1}{2}\pi\rangle$, while curves $\tilde{E}_{e\pm}^2(\theta; y)$ are

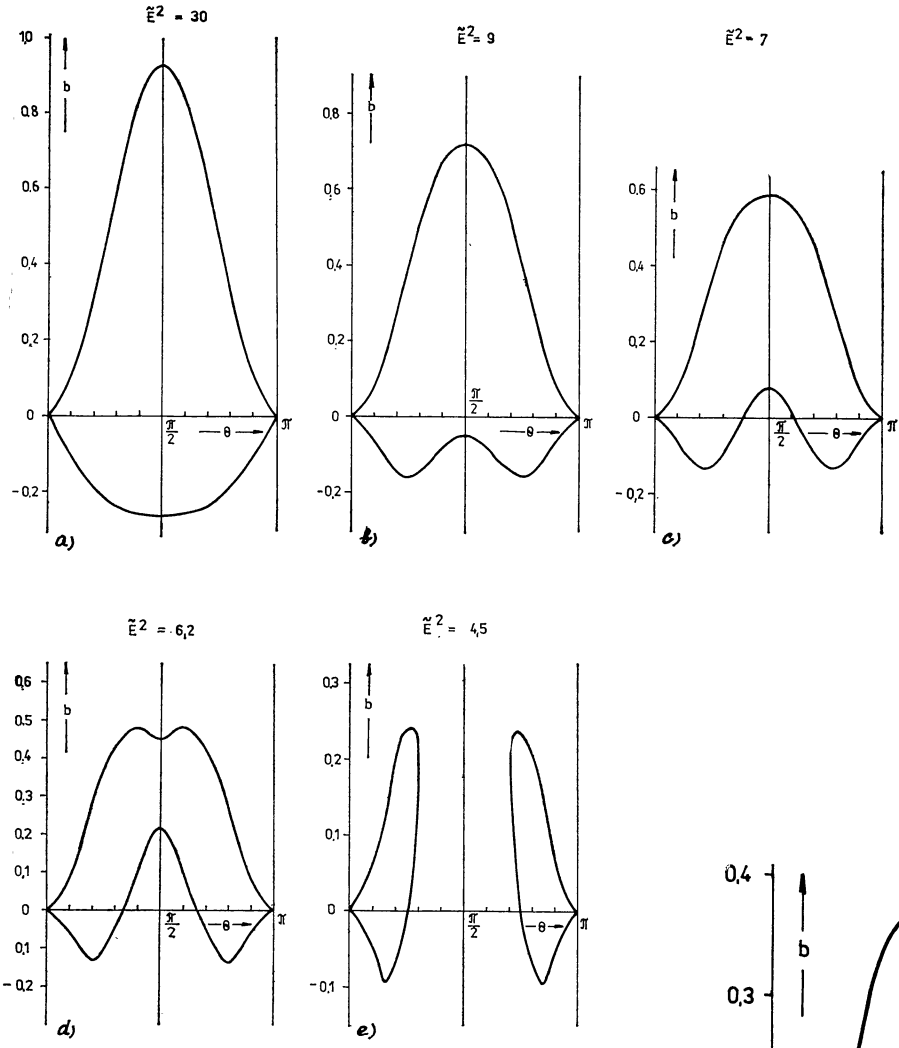

Fig. 18. Sequence of figures showing typical behaviour of the curves $b_{e\pm}(\theta; \tilde{E}^2, y)$ for $y \in (-1, -0{\cdot}2956)$. The sequence is plotted for $y = -0{\cdot}5$ and is labelled by values of $\tilde{E}^2$ for which the figures are drawn.

defined at $\theta \in \langle \theta_e, \frac{1}{2}\pi \rangle$, where θ_r and θ_e are given by (28) and (24); recall that $\theta_r < \theta_e$. At θ_e it is $\tilde{E}_r^2(\theta_e) = \tilde{E}_{e\pm}^2(\theta_e) = -(1 + y)^{-1}$. The situation is demonstrated in Fig. 24 – these curves have no common point except that at $\theta = \theta_e$.

There are five ranges of parameter $\tilde{E}^2$ which determine the corresponding five types of behaviour of $b_{e\pm}(\theta; \tilde{E}, y)$:

a) $\tilde{E}^2 > \tilde{E}_{e-}^2(\frac{1}{2}\pi)$,

b) $\tilde{E}_{e-}^2(\frac{1}{2}\pi) > \tilde{E}^2 > \tilde{E}_{e+}^2(\frac{1}{2}\pi)$,

c) $\tilde{E}_{e+}^2(\frac{1}{2}\pi) > \tilde{E}^2 > \tilde{E}_r^2(\frac{1}{2}\pi)$,

d) $\tilde{E}_r^2(\frac{1}{2}\pi) > \tilde{E}^2 > \tilde{E}_{e\pm}^2(\theta_e)$,

e) $\tilde{E}_{e\pm}^2(\theta_e) > \tilde{E}^2 > 0$.

One can see immediately that for any value of $\tilde{E}^2 > 0$ curves $b_{e\pm}(\theta; \tilde{E}, y)$ cover all the range $(-\infty,$

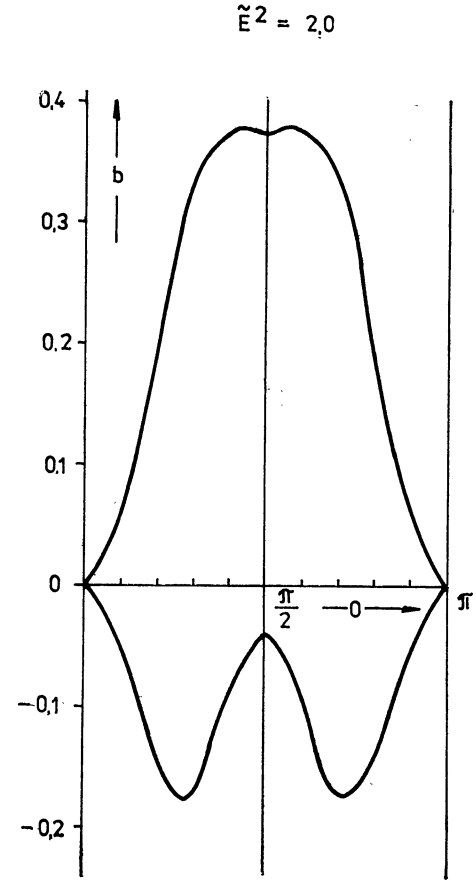

Fig. 19. Behaviour of the curves $b_{e\pm}(\theta; \tilde{E}^2, y)$ for $y \in \in (-0{\cdot}2956, 0)$ in the case when Fig 18c is irrelevant; in other cases Figs 18a, b, d, e are valid. The figure is plotted for $y = -2$, $\tilde{E}^2 = 2$.

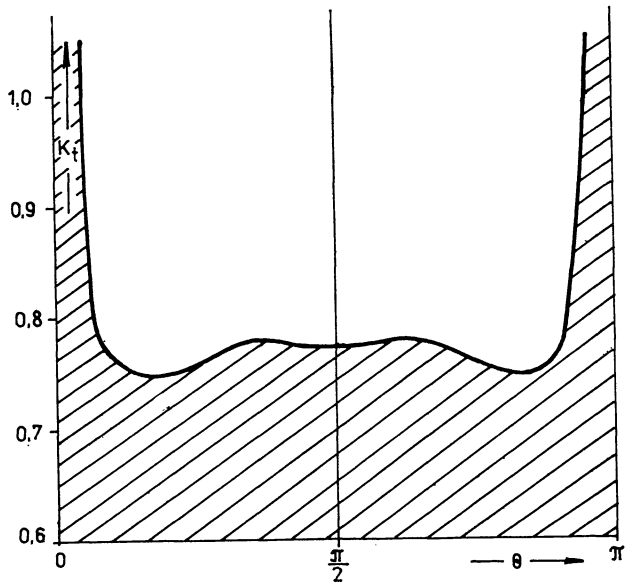

Fig. 20. K_t-section for $y = -0{\cdot}2$, $\tilde{E}^2 = 2$, $\mathsf{b} = -0{\cdot}1$. In this case unstable $\theta = \text{const} \neq \frac{1}{2}\pi$ trajectories occur beside the stable $\theta = \text{const}$ orbits.

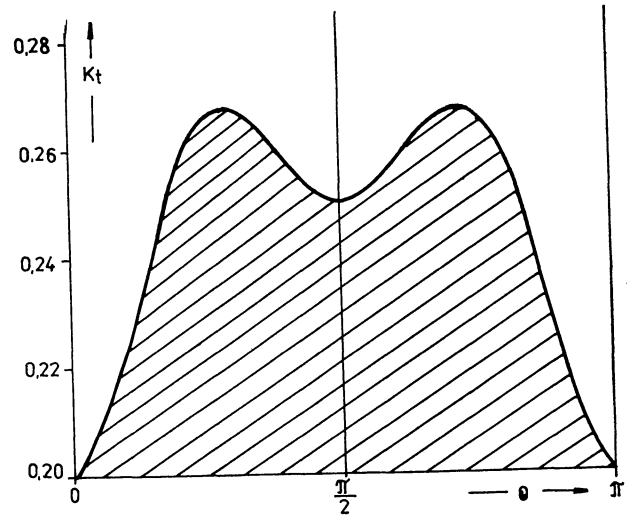

Fig. 21. K_t-section in the special case $b = 0$ (for $y = -0{\cdot}5$, $\tilde{E}^2 = 5$).

$+\infty$), and for $\tilde{E}^2 > -(1+y)^{-1}$ they are always defined at $\theta \in \langle 0, \theta_e \rangle$ – in this interval curves $\mathsf{b}_{e\pm}(\theta; \tilde{E}, y)$ determine maxima of K_t-sections, if $\mathsf{b} \neq (y+1)/y$, and $\mathsf{b} \neq 0$.

If a line $\mathsf{b} = \text{const} \neq (y+1)/y \neq 0$ has no intersection with $\mathsf{b}_{e\pm}(\theta; \tilde{E}, y)$ at $\theta \in (\theta_e, \frac{1}{2}\pi)$, the behaviour of K_t-sections is depicted in Fig. 9, if there is one intersection at $\theta \in (\theta_e, \frac{1}{2}\pi)$ the section of $K_t(\theta; \tilde{E}, y)$ is characterized in Fig. 10 (with $K_{t\min} > 0$), and for two points of intersection at $\theta \in (\theta_e, \frac{1}{2}\pi)$ the behaviour of K_t-sections is given in Fig. 26 – then one stable and one unstable $\theta = \text{const}$ trajectories are possible

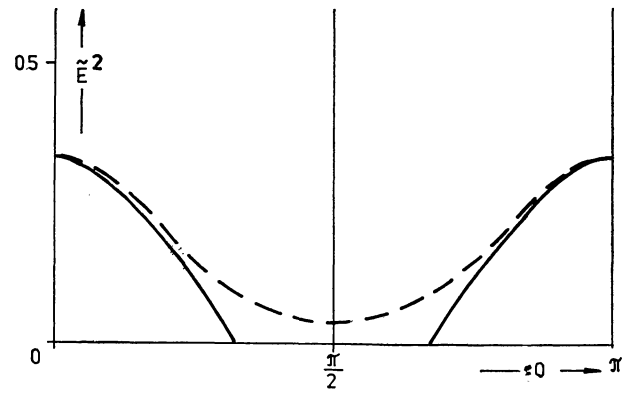

Fig. 22. Behaviour of the curves $\tilde{E}_r^2(\theta; y)$ (solid curve) $\tilde{E}_z^2(\theta; y)$ (dashed curve) in the $y > 1$ case. The figure is plotted for $y = 2$.

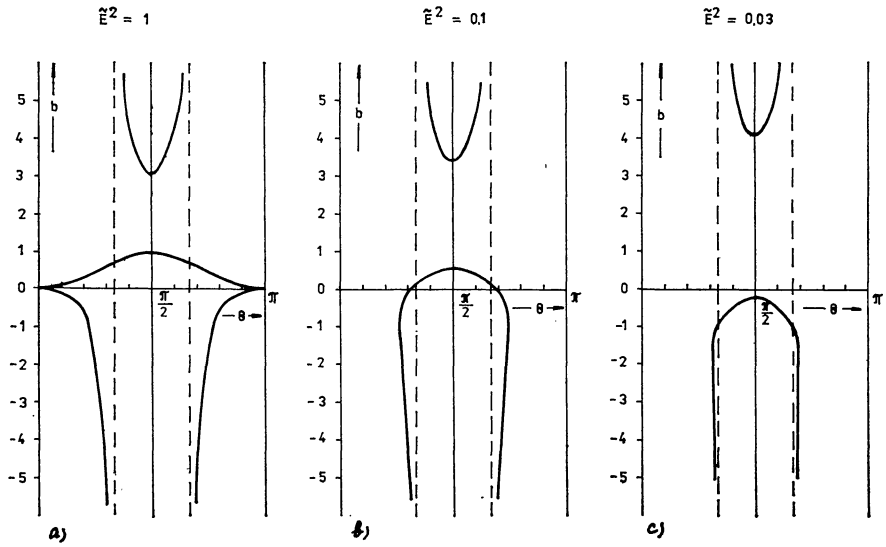

Fig. 23. Sequence of figures giving typical behaviour of curves $\mathsf{b}_{e\pm}(\theta; \tilde{E}^2, y)$ for $y > 1$. The sequence is given for $y = 2$, and is labelled by values of $\tilde{E}^2$ for which the figures are drawn.

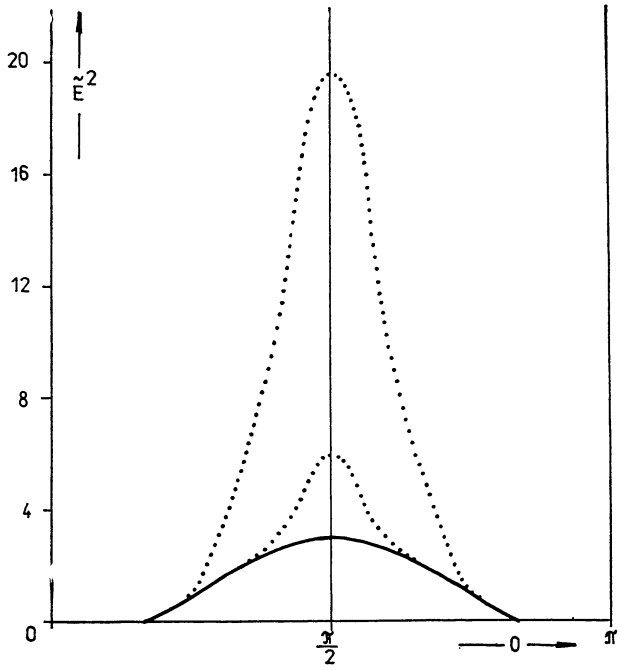

Fig. 24. Behaviour of the curves $\tilde{E}^2_r(\theta; y)$ (solid curve), $\tilde{E}^2_{e\pm}(\theta; y)$ (dotted curves) in the $y < -1$ case. The figures are drawn for $y = -2$.

at $\theta \in (\theta_e, \frac{1}{2}\pi)$, note that this situation can arise only if $(1+y)^{-4}[1 - y^3 - 2y(-y)^{1/2}] > \tilde{E}^2 > -(1+y)^{-1}$ (see Figs 25b–d). Further information can straightforwardly be read out from Fig. 25.

For $b = 0$ and any $\tilde{E}^2 > 0$ the K_t-section is characterized by Fig. 12. If $b = (y + 1)/y$, we obtain two possibilities for the behaviour of K_t-sections: that of Fig. 11 for $\tilde{E}^2 > (1 - y)/(1 + y)^2$, and that of Fig. 27 for $\tilde{E}^2 < (1 - y)/(1 + y)^2$.

There is one important feature of the latitudinal motion in the case $y < -1$: no test particle can cross the barrier at $\theta = \theta_e$ hyperboloid which is the singularity of the metric coefficient Δ_θ.

Finally we can conclude that for repulsive cosmological constant the latitudinal motion in the Kerr-de Sitter metric has similar character as in the Kerr metric, while for the attractive cosmological constant new feature arises as unstable θ = const trajectories can exist outside the equatorial plane in addition to the stable trajectories. The presented analysis is valid also for latitudinal motion of electrically charged test particles in the Kerr-Newman-de Sitter spacetime with $P = 0$.

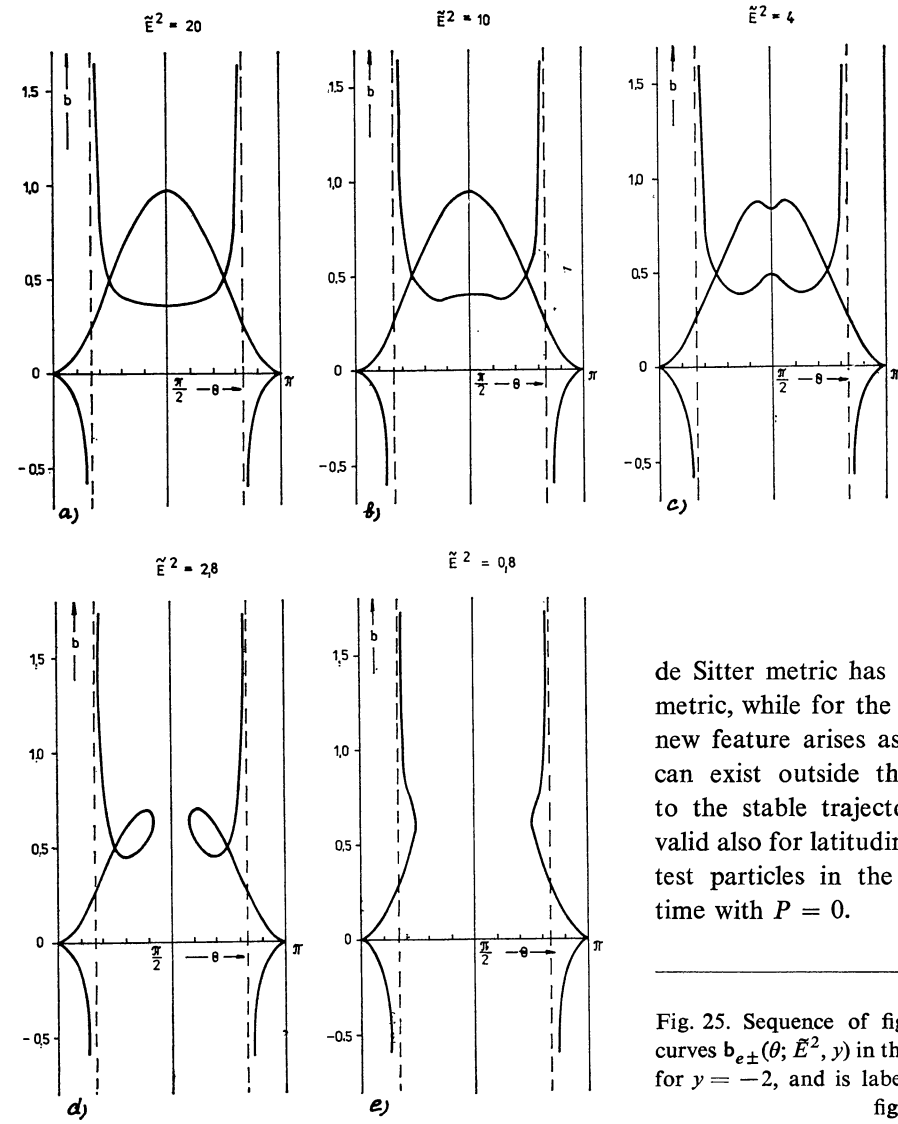

Fig. 25. Sequence of figures determining behaviour of the curves $b_{e\pm}(\theta; \tilde{E}^2, y)$ in the $y < -1$ case. The sequence is given for $y = -2$, and is labelled by values of $\tilde{E}^2$ for which the figures are drawn.

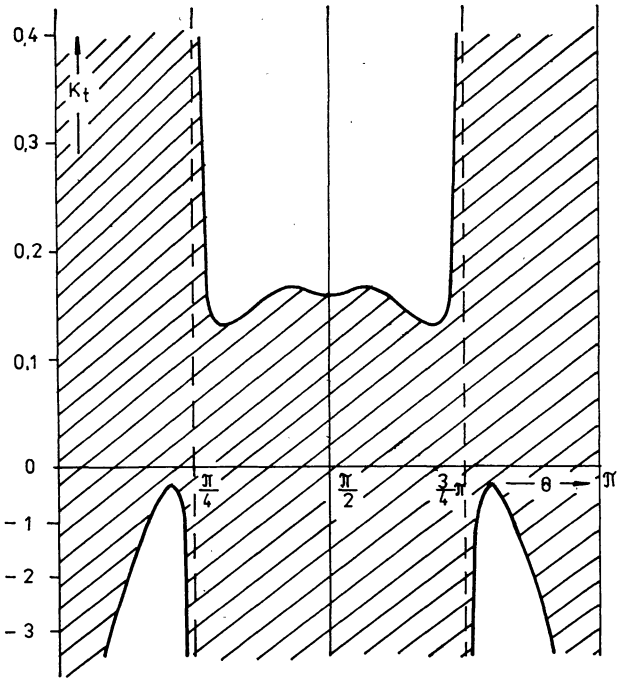

Fig. 26. K_t-section for $y = -2$, $\tilde{E}^2 = 2{\cdot}8$, $b = 0{\cdot}6$. Again, unstable $\theta = \text{const} \neq \frac{1}{2}\pi$ trajectories exist.

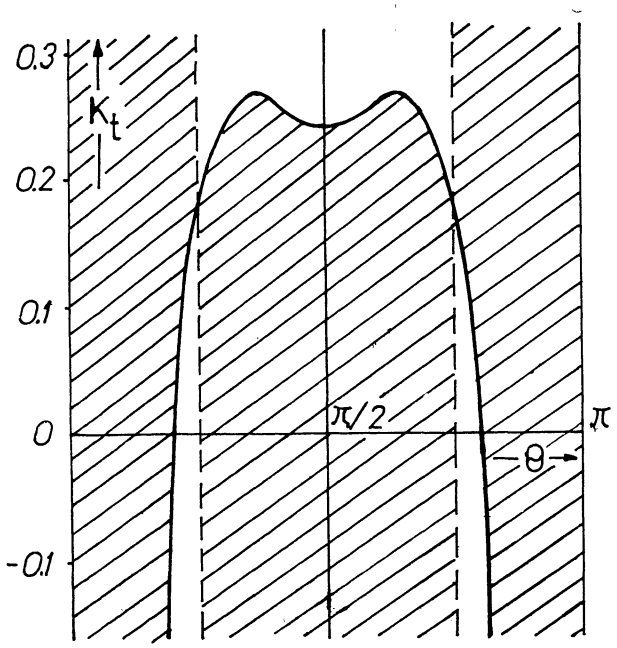

Fig. 27. K_t-section in the special case $b = (y+1)/y$ for $y < -1$. The figure is plotted for $y = -2$, $\tilde{E}^2 = 2{\cdot}8$, $b = 0{\cdot}5$.

4. The Radial Motion of Test Particles in the Schwarzschild-de Sitter Spacetime

The radial motion of charged test particles in the most general Kerr-Newman-de Sitter dyon spacetime is governed by Eq. (10), where expression R can be written as

$$R = \tfrac{1}{3}\Lambda m^2 r^6 + \\ + [I^2E^2 - m^2(1 - \tfrac{1}{3}a^2\Lambda + \tfrac{1}{3}\Lambda\mathcal{K}]r^4 + \\ + 2(IeQE + m^2M)\,r^3 + \\ + [2I^2aE(aE - \Phi) + e^2Q^2 - m^2(a^2 + Q^2) - \\ - (1 - \tfrac{1}{3}a^2\Lambda)\,\mathcal{K}]\,r^2 + 2(Ia^2QeE + M\mathcal{K})\,r + \\ + I^2a^2(aE - \Phi)^2 - (a^2 + Q^2)\,. \tag{41}$$

From (41) it is clear that for a repulsive cosmological term ($\Lambda > 0$) infinity can be reached by particles with arbitrary value of the energy parameter E (recall that for $\Lambda = 0$ only particles with $E \geqq m$ can escape to infinity) for both nonzero and zero rest mass particles.

On the other hand, for an attractive cosmological term ($\Lambda < 0$) no particle with $m \neq 0$ can reach infinity by following a geodesic trajectory – see also Hawking and Ellis (1973) where this is exhibited in the conformal diagram of the anti-de Sitter spacetime. A particle with $m = 0$ can escape to infinity if its energy parameter E satisfies the condition

$$E^2 \geqq -\frac{\Lambda}{3I^2}\mathcal{K}\,.$$

A more detailed discussion of radial motion in the most general background (2) is very difficult due to the great complexity of (41). Therefore we restrict our attention to the much simpler case of the Schwarzschild-de Sitter spacetime

$$\mathrm{d}s^2 = -(1 - 2M/r - \tfrac{1}{3}\Lambda r^2)\,\mathrm{d}t^2 + \\ + (1 - 2M/r - \tfrac{1}{3}\Lambda r^2)^{-1}\,\mathrm{d}r^2 + r^2(\mathrm{d}\theta^2 + \sin^2\theta\,\mathrm{d}\varphi^2)\,, \tag{42}$$

as the metric describes the simplest black-hole asymptotically de Sitter background.

If $\Lambda < 0$, the metric (42) has only one apparent singularity (horizon) which is located at

$$r_h = \left[-\frac{3M}{\Lambda} + \left(\frac{9M^2}{\Lambda^2} - \frac{1}{\Lambda^3}\right)^{1/2}\right]^{1/3} + \\ + \left[-\frac{3M}{\Lambda} - \left(\frac{9M^2}{\Lambda^2} - \frac{1}{\Lambda^3}\right)^{1/2}\right]^{1/3}. \tag{43}$$

One can show that $0 < r_h < 2M$; for $\Lambda = 0$ we arrive at the well known results $r_h = 2M$. If $\Lambda > 0$ we obtain three well defined cases. For $9M^2\Lambda < 1$ there are three distinct apparent singularities of (42) the loci of which are at

$$r_u = -2\Lambda^{-1/2}\cos\tfrac{1}{3}\psi\,, \tag{44a}$$

$$r_h = 2\Lambda^{-1/2}\cos(\tfrac{1}{3}\pi + \tfrac{1}{3}\psi)\,, \tag{44b}$$

$$r_c = 2\Lambda^{-1/2}\cos(\tfrac{1}{3}\pi - \tfrac{1}{3}\psi)\,, \tag{44c}$$

where

$$\psi = \arccos(3M\Lambda^{1/2})\,. \tag{45}$$

As the inequality $2M < r_h < 3M < r_c$ is satisfied we can say that r_h is the black-hole horizon, and r_c is the cosmological horizon; since $r_u < 0$, it is an unrealistical apparent signularity, as the physical singularity at $r = 0$ (which is present for any values of Λ, and $M \neq 0$) is inevitable in the spherically symmetric Schwarzschild case. (The conformal diagram of the Schwarzschild-de Sitter spacetime in the case $9M^2\Lambda < 1$ is given in Gibbons and Hawking, 1977 – there is an infinite sequence of singularities $r = 0$ and spacelike infinities $r = \infty$.) When $9M^2\Lambda = 1$ the horizons r_h and r_c coalesce at

$$r_d = \Lambda^{-1/2} = 3M . \tag{46}$$

For $9M^2\Lambda > 1$ only the unrealistic apparent singularity $r_u < 0$ remains, which is now determined by (43).

The equations of geodesic motion in the Schwarzschild-de Sitter background are governed by Eqs (10)–(17) with $a = Q = 0$. Due to the spherical symmetry of the background the motion can always be considered in the equatorial plane $(\theta = \frac{1}{2}\pi)$ – the latitudinal equation (11) then yields $\mathrm{d}\theta/\mathrm{d}\lambda = 0$ as $\mathscr{K} = L^2$ (L is a constant corresponding to the total angular momentum of the particle motion) in spherically symmetric backgrounds and for the motion in the equatorial plane there is $L^2 = \Phi^2$.

The character of the radial motion can conveniently be clarified by properties of circular orbits and purely radial trajectories. The radial motion is determined by Eq. (10), and for Schwarzschild-de Sitter spacetime given by

$$R = r\left[\tfrac{1}{3}\Lambda m^2 r^5 + \right. \tag{47}$$
$$\left. + (E^2 - m^2 + \tfrac{1}{3}\Lambda\Phi^2) r^3 + 2m^2 M r^2 - \Phi^2 r + 2M\Phi^2\right].$$

a) Circular Orbits

For a circular orbit with radius r the conditions

$$R(r) = 0 , \tag{48}$$

and

$$\mathrm{d}R(r)/\mathrm{d}r = 0 \tag{49}$$

must be satisfied simultaneously. By solving eqs (48) and (49) with respect to the constants of motion E, Φ, one finds that for a circular orbit at a given r test particles must have constants of motion determined by the conditions

$$E/m = (1 - 2M/r - \tfrac{1}{3}\Lambda r^2)(1 - 3M/r)^{-1/2} , \tag{50}$$

$$\Phi/m = \pm[r(M - \tfrac{1}{3}\Lambda r^3)]^{1/2}(1 - 3M/r)^{-1/2} ; \tag{51}$$

only particles in positive-root states (see e.g. Misner et al., 1973) are considered.

Equations (50) and (51) impose the following restrictions on the existence of circular orbits:

$$r \geqq 3M , \quad r \leqq (3M/\Lambda)^{1/3} , \tag{52}$$

if $\Lambda > 0$. For $\Lambda < 0$ circular orbits do exist for all $r \geqq 3M$. From (52) it is clear that for $9M^2\Lambda = 1$ only circular null orbits, which are located at the degenerate horizon r_d, are possible, while for $9M^2\Lambda > 1$ there are no circular orbits at all.

Unstable circular null orbits with "impact" parameter

$$l \equiv \frac{\Phi}{E} = \frac{3^{3/2}M}{(1 - 9M^2\Lambda)^{1/2}} \tag{53}$$

are located at $r = 3M$. (Notice that the radius of the circular orbits of photons, if defined, is not effected by the cosmological constant explicitly.)

The stability condition of circular orbits with respect to perturbations in the r-direction is

$$\mathrm{d}^2R(r)/\mathrm{d}r^2 \leqq 0 . \tag{54}$$

By solving (54) with E/m and Φ/m given by (51), (50) we arrive at condition

$$\tfrac{4}{3}\Lambda r^4 - 5M\Lambda r^3 - Mr + 6M^2 \leqq 0 , \tag{55}$$

which determines the loci of stable circular orbits in the background with given M, Λ. (The equality in (54) and (55) holds for marginally stable orbits.) Notice that (55) can be considered as a quadratic expression in M and, therefore, the stable orbits do exist for

$$M(r; \Lambda) < M < M_+(r; \Lambda) . \tag{56}$$

where

$$M_\pm(r; \Lambda) = \tfrac{1}{12}r(5\Lambda r^2 + 1 \pm B^{1/2}) \tag{57}$$

with

$$B = 25\Lambda^2 r^4 - 22\Lambda r^2 + 1 . \tag{58}$$

If $\Lambda > 0$, curves $M_\pm(r; \Lambda)$ are defined for $r < r_1$, and $r > r_2$, where

$$r_1 = \frac{1}{\Lambda^{1/2}}\left[\frac{22 - 384^{1/2}}{50}\right]^{1/2} \doteq \frac{0{\cdot}2193}{\Lambda^{1/2}} , \tag{59a}$$

$$r_2 = \frac{1}{\Lambda^{1/2}}\left[\frac{22 + 384^{1/2}}{50}\right]^{1/2} \doteq \frac{0{\cdot}9121}{\Lambda^{1/2}} . \tag{59b}$$

Nevertheless, one can show that curves $M_\pm(r; \Lambda)$ determine stable circular orbits only if $r < r_1$, while they are irrelevant at $r > r_2$. Why? Because the restrictive conditions (52) and $9M^2\Lambda < 1$ on the existence of circular orbits must be taken into account; there is the point of intersection of curves $M_-(r; \Lambda)$, $M = r/3$, $M = r^3/(3\Lambda)$ at $r = \Lambda^{-1/2}$, where condition $9M^2\Lambda = 1$ is satisfied – as $M_\pm(r_2; \Lambda) > r_2/3$, curves $M_\pm$

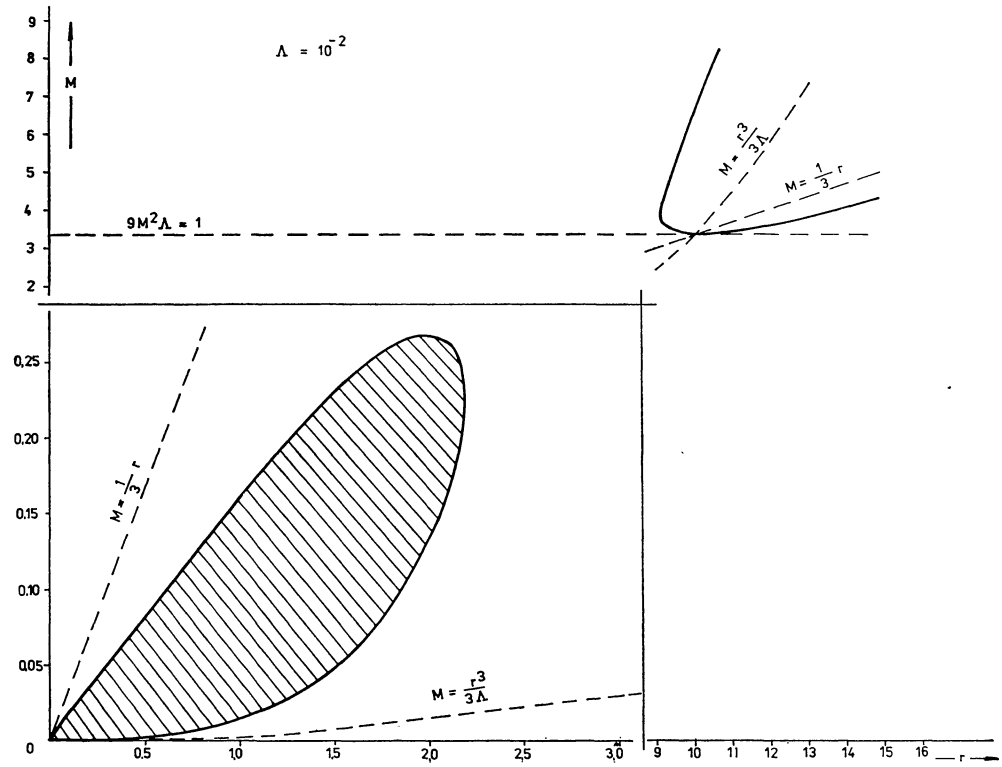

Fig. 28. Stable circular orbits in Schwarzschild-de Sitter spacetime with repulsive Λ-term. The parameter M and radii r are both given in units of length, and the cosmological constant is given in units of (length)$^{-2}$. Circular orbits occur at $M \leqq \frac{1}{3}r$ and $M \geqq \frac{1}{3}r^3/\Lambda$, while the stable orbits are possible in the shaded region only. Thus the existence of stable orbits is limited in values of both radii r and the mass parameter M.

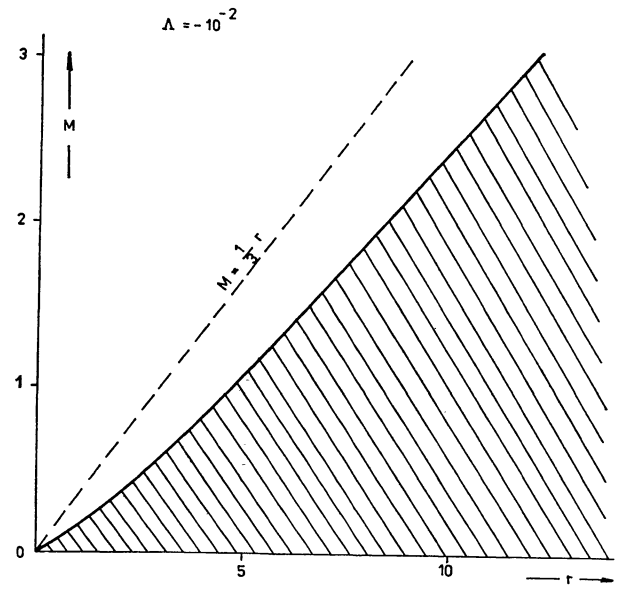

Fig. 29. Stable circular orbits in Schwarzschild-de Sitter spacetime with attractive Λ-term. The parameter M and radii r are both given in units of length, and the cosmological constant is given in units of (length)$^{-2}$. Existence of circular orbits is restricted by condition $M \leqq \frac{1}{3}r$ only, the stable orbits are allowed in the shaded region — stable orbits can exist for all values of the mass parameter M.

$(r; \Lambda)$ do not satisfy the restrictions (52) if $r > r_2$ — see Fig. 28.

From Fig. 28 it is clear that the existence of stable orbits is restricted not only for the radii $(r < r_1)$, but also for the mass parameter M. There are no stable circular orbits if $M > M_{\text{crit}}(\Lambda)$, where $M_{\text{crit}}(\Lambda)$ is the value of the curve $M_+(r; \Lambda)$ at its maximum.

On the other hand, for $\Lambda < 0$ curves $M_\pm(r; \Lambda)$ are defined for all values of r, and stable orbits exist for all values of M — see Fig. 29.

b) *Radial Trajectories*

For purely radial trajectories we have $\Phi = 0$, and (47) is simplified to

$$R = m^2 r^3 (\tfrac{1}{3}\Lambda r^3 + \Gamma r + 2M), \tag{60}$$

where new constant of motion

$$\Gamma = \tilde{E}^2 - 1 \tag{61}$$

has been introduced. By using (10) the radial trajectories can be given in terms of the proper time of test particles with $m \neq 0$:

$$\mathrm{d}\tau = \frac{\pm r\,\mathrm{d}r}{[r(\tfrac{1}{3}\Lambda r^3 + \Gamma r + 2M)]^{1/2}}; \tag{62}$$

note that for purely radial photons we have

$$d\lambda = \pm \frac{dr}{E}. \tag{62'}$$

The radial trajectories can also be given in terms of the coordinate time t; from (10) and (13) we obtain

$$dt = \frac{\pm \tilde{E} r^2 \, dr}{(\frac{1}{3}\Lambda r^3 + r - 2M)\left[r(\frac{1}{3}\Lambda r^3 + \Gamma r + 2M)\right]^{1/2}}. \tag{63}$$

In (62) and (63) the + sign corresponds to outgoing geodesics, and the − sign gives ingoing geodesics.

First, turning points of the radial trajectories must be found. The loci of turning points are determined by non-negative roots of (60). There is always a root of (60) at $r = 0$ where the physical singularity of Schwarzschild-de Sitter spacetimes is located − thus outgoing geodesics can originate at the past singularity, while ingoing geodesics can terminate at the future singularity. The other roots of (60) will be discussed in dependence on Λ:

i) $\Lambda > 0$

If $9M^2\Lambda \geqq 1$, no turning points of radial geodesics are possible. Therefore, attention will be devoted to the case $9M^2\Lambda < 1$, when two horizons are present. If $\Gamma < -(3M)^{2/3}\Lambda^{1/3}$ (recall that $\Gamma \geqq -1$ always), then (60) yields two turning points

$$r_{t1} = 2(-\Gamma/\Lambda)^{1/2} \cos(\tfrac{1}{3}\pi + \tfrac{1}{3}\zeta), \tag{64a}$$

$$r_{t2} = 2(-\Gamma/\Lambda)^{1/2} \cos(\tfrac{1}{3}\pi - \tfrac{1}{3}\zeta), \tag{64b}$$

where

$$\zeta = \arccos \frac{3M\Lambda^{1/2}}{(-\Gamma)^{3/2}}. \tag{65}$$

Thus in this case there are two possibilities − in the first one geodesics originate at the past $r = 0$ singularity, have a turning point at r_{t1} and terminate in the future $r = 0$ singularity, in the second one geodesics are ingoing from the past infinity and from the turning point r_{t2} are outgoing to the future infinity (see e.g. the conformal diagram of the Schwarzschild-de Sitter metric in Gibbons and Hawking, 1977). One can easily show that both the turning points must be located between the black-hole (r_h) and the cosmological (r_c) horizons. This in fact becomes clear immediately if we rewrite Eq. (10) in the form

$$(dr/d\tau)^2 + V_{ef} = \tilde{E}^2$$

with

$$V_{ef} = (1 - 2M/r - \tfrac{1}{3}\Lambda r^2).$$

If $\Gamma = -(3M)^{2/3}\Lambda^{1/2}$, we obtain a static radius

$$r_s = (3M/\Lambda)^{1/3}. \tag{66}$$

Notice that r_s imposes the upper restriction on the existence of circular orbits − see (52). For a particle at the static radius the attraction of the mass M is just compensated by the repulsion of the cosmological Λ-term − from (51) we have $\Phi/m = 0$ − while for circular orbits the attractive effect of M is compensated by repulsive effects of both the Λ-term and the orbital motion. Particles at the static radius are in unstable equilibrium (there is a maximum of the effective potential V_{ef} at r_s) so that any perturbation causes them to escape to infinity or to fall into the $r = 0$ singularity.

If $\Gamma > -(3M)^{2/3}\Lambda^{1/3}$, there are no turning points and therefore only geodesics ingoing from past infinity to the future $r = 0$ singularity or outgoing from the past $r = 0$ singularity to the future infinity are possible.

ii) $\Lambda < 0$

For radial timelike geodesics one turning point must always exist, while all purely radial photons can escape to infinity − see (62), (62').

If $0 < \Gamma < -(3M)^{2/2}\Lambda^{1/3}$ the turning point is given by

$$r_t = [-3M/\Lambda + (9M^2/\Lambda^2 + \Gamma^3/\Lambda^3)^{1/2}]^{1/3} + [-3M/\Lambda - (9M^2/\Lambda^2 + \Gamma^3/\Lambda^3)^{1/2}]^{1/3}, \tag{67}$$

while for $\Gamma > -(3M)^{2/3}\Lambda^{1/3}$ it is determined by

$$r_t = 2(-\Gamma/\Lambda)^{1/2} \cos \tfrac{1}{3}\xi, \tag{68}$$

where

$$\xi = \arccos [3M(-\Lambda)^{1/2}\Gamma^{-3/2}],$$

and for $\Gamma < 0$ we arrive at

$$r_t = 2(-\Gamma/\Lambda)^{1/2} \cosh \tfrac{1}{3}\xi', \tag{69}$$

where

$$\xi' = \operatorname{arccosh} [3M(-\Lambda)^{1/2}\Gamma^{-3/2}].$$

Equations (62) and (63) can be integrated and given in terms of elliptic integrals in all cases discussed above. Here we shall consider in detail only the case $\Lambda > 0$, $9M^2\Lambda < 1$, $\Gamma < -(3M)^{2/3}\Lambda^{1/3}$ when two horizons and two turning points are present. According to Gradstein and Ryzhik (1971) we find that for a particle which originates at the $r = 0$ singularity and from r_{t1} returns to $r = 0$ it is

$$\tau(r) = \pm \left(\frac{3}{\Lambda}\right)^{1/2} \frac{2}{[r_{t2}(r_{t1} - r_{tu})]^{1/2}} \times \times \left\{(r_{t1} - r_{t2}) \Pi\left(\varkappa, \frac{r_{t1}}{r_{t2}}, \tilde{l}\right) + r_{t2} F(\varkappa, \tilde{l})\right\}, \tag{70}$$

and

$$t(r) = \pm \tilde{E}(3/\Lambda)^{3/2} \times \sum^{\alpha} A_\alpha I_\alpha, \tag{71}$$

where

$$(72)\quad I_\alpha = \frac{2}{(r_\alpha - r_{t2})(r_\alpha - r_{t1})[r_{t2}(r_{t1} - r_{tu})]^{1/2}} \times \left\{(r_{t1} - r_{t2}) \Pi\left(\varkappa, \frac{r_{t1}(r_\alpha - r_{t2})}{r_{t2}(r_\alpha - r_{t1})}, \tilde{l}\right) + (r_\alpha - r_{t1}) F(\varkappa, \tilde{l})\right\};$$

here $\alpha = c, h, u$. The parameters of the elliptic integrals are given by the following formulas

$$(70')\quad \varkappa = \arcsin\left[\frac{r_{t2}(r_{t1} - r)}{r_{t1}(r_{t2} - r)}\right]^{1/2},$$

$$(70'')\quad \tilde{l} = \left[\frac{r_{t1}(r_{t2} - r_{tu})}{r_{t2}(r_{t1} - r_{tu})}\right]^{1/2},$$

and the unrealistic turning point r_{tu} is determined by

$$(70''')\quad r_{tu} = -2(-\Gamma/\Lambda)^{1/2} \cos \tfrac{1}{3}\zeta .$$

The constants A_α are given in the following manner:

$$(71')\quad A_c = \frac{r_c^2}{(r_c - r_u)(r_c - r_h)},$$

$$A_h = \frac{r_h^2}{(r_h - r_c)(r_h - r_u)}, \quad A_u = \frac{r_u^2}{(r_u - r_c)(r_u - r_h)}.$$

At $r = r_h$ we find that $t \to -\infty$ for outgoing geodesics, and $t \to +\infty$ for ingoing geodesics – compare this situation with Fig. 31.1 in Misner et al. (1973).

For a particle which originates at infinity with the same parameter Γ and from r_{t2} returns to infinity we arrive at

$$(73)\quad \tau(r) = \pm\left(\frac{3}{\Lambda}\right)^{1/2} \frac{2}{[r_{t2}(r_{t1} - r_{tu})]^{1/2}} \times \left\{(r_{t2} - r_{t1}) \Pi\left(v, \frac{r_{t2} - r_{tu}}{r_{t1} - r_{tu}}, \tilde{l}\right) + r_{t1} F(v, \tilde{l})\right\},$$

and

$$(74)\quad t(r) = \pm \tilde{E}(3/\Lambda)^{3/2} \times \sum^{\alpha} A_\alpha \tilde{I}_\alpha ,$$

where

$$(75)\quad \tilde{I}_\alpha = \frac{2}{(r_\alpha - r_{t2})(r_\alpha - r_{t1})[r_{t2}(r_{t1} - r_{tu})]^{1/2}} \times \left\{(r_{t2} - r_{t1}) \Pi\left(v, \frac{(r_{t2} - r_{tu})(r_\alpha - r_{t1})}{(r_{t1} - r_{tu})(r_\alpha - r_{t2})}, \tilde{l}\right) + (r_\alpha - r_{t2}) F(v, \tilde{l})\right\}.$$

The parameter v is given by

$$(73')\quad v = \arcsin\left[\frac{(r_{t1} - r_{tu})(r - r_{t2})}{(r_{t2} - r_{tu})(r - r_{t1})}\right]^{1/2}.$$

In this case we obtain that at $r = r_c$ $t \to +\infty$ for outgoing geodesics, and $t \to -\infty$ for ingoing geodesics; at infinity $t = 0$ for both ingoing and outgoing geodesics.

Note that the integrals (70)–(75) are chosen to yield $\tau = 0$ and $t = 0$ at both r_{t1} and r_{t2}, respectively.

If $\Gamma > -(3M)^{2/3} \Lambda^{1/2}$ (no turning points present) the expressions for τ and t become quite complicated. Therefore as an illustration we shall only give the expression for the proper time of a particle with $\Gamma > 0$ which is outgoing from the $r = 0$ singularity to infinity: at $r \leqq q$ the proper time is determined by

$$(76)\quad \tau(r) = \mathscr{I}_1 - \mathscr{I}_2 ,$$

where

$$(77a)\quad \mathscr{I}_1 = -\frac{(pP_1 + qM_1)(p - q)}{(p_1 + M_1)(PM_1 - MP_1)^{1/2}} F(\iota, \tilde{h}) + \frac{(p - q)^2 P_1}{(P_1 + M_1)(PM_1 - MP_1)^{1/2}} \times \Pi\left(\iota, \tilde{h}^2\left(1 + \frac{P_1}{M_1}\right), \tilde{h}\right),$$

$$(77b)\quad \mathscr{I}_2 = -\frac{(p - q)^2}{2(-MM_1\tilde{C})^{1/2}} \times \ln\left|2\left[\frac{\tilde{C}(Mz + P)(M_1 z + P_1)}{(z - 1)^2}\right]^{1/2} + \frac{2\tilde{C}}{z - 1} + \tilde{B}\right|.$$

The parameters of the elliptic integrals are

$$(77')\quad \iota = \arcsin\left[\left(1 - \frac{MP_1}{M_1 P}\right)\frac{M_1 z}{M_1 z + P_1}\right]^{1/2},$$

$$\tilde{h} = \left(\frac{M_1 P}{M_1 P - MP_1}\right)^{1/2},$$

and the coefficients and the variable z are given by the following relations:

$$(77'')\quad z = \left(\frac{r - q}{p - r}\right)^2,$$

$$q = \frac{1}{4}\frac{\tilde{n}^2}{\tilde{m}}(1 + \tilde{D}^{1/2}), \quad p = \frac{1}{4}\frac{\tilde{n}^2}{\tilde{m}}(1 - \tilde{D}^{1/2}),$$

where

$$\tilde{m} = (\Gamma/\Lambda)^{1/2} \sinh \tfrac{1}{3}\beta ,$$

$$\tilde{n}^2 = (\Gamma/\Lambda)(\sinh^2 \tfrac{1}{3}\beta + 3\cosh^2 \tfrac{1}{3}\beta),$$

$$\tilde{D} = 1 + \frac{8 \sinh^2 \tfrac{1}{3}\beta}{4 \cosh^2 \tfrac{1}{3}\beta - 1},$$

$$\beta = \operatorname{arcsinh}\left[3M\Lambda^{1/2}\Gamma^{-3/2}\right];$$

further

$$M = p(p + 2\tilde{m}), \quad M_1 = p(p - 2\tilde{m}) + \tilde{n}^2,$$
$$P = q(q + 2\tilde{m}), \quad P_1 = q(q - 2\tilde{m}) + \tilde{n}^2,$$

and

$$\tilde{B} = 2MM_1 + M_1P + MP_1 ,$$
$$\tilde{C} = (M + P)(M_1 + P_1) .$$

At $r \geqq q$ the proper time of the particle is given by

(78) $$\tau(r) = \mathscr{I}_1 + \mathscr{I}_2 + \tilde{K} ,$$

where the constant of integration must be chosen as

(79) $$\tilde{K} = -\frac{(p-q)^2}{(-MM_1\tilde{C})^{1/2}} \ln \left| 2(\tilde{C}PP_1)^{1/2} - 2\tilde{C} + \tilde{B} \right| .$$

5. A Possibility of Constructing a Model of the Einstein-Strauss-de Sitter Universe

The Einstein-Strauss universe is referred to as a model of Schwarzschild condensations immersed in a dust Friedman cosmological model (see Jantzen and Ruffini, 1981). It is the simplest approximation to the problem of localized mass distribution in our Universe.

In the Einstein-Strauss universe, the Schwarzschild vacuum solution is smoothly matched on a time-dependent outgoing (or ingoing in the collapsing universe) sphere to a co-moving sphere of cosmological fluid in the dust Friedman model. Thus the interior of a spherical shell S_F of cosmological fluid in dusty Friedman spacetime is replaced by the interior of a spherical tube S_S in a Schwarzschild spacetime. (Here the Schwarzschild geometry is combined with a Friedman exterior; in the model of gravitational collapse of a dusty star – see e.g. Misner et al. (1973) – Schwarzschild geometry is matched to a Friedman interior, but the matching conditions are identical in both cases.)

As for dust particles in S_F all spatial Friedman coordinates are constant, the particles must move along timelike radial geodesics in S_S, if S_F and S_S are identified. The matching is possible only if the proper times on the geodesics in S_F and S_S can be synchronized in such a manner that the circumferences of S_F and S_S are the same at corresponding proper times – see Jantzen and Ruffini (1981) and references therein.

Here we shall show that the synchronization of proper times is possible also in the case of matching of Schwarzschild-de Sitter spacetime to dust Friedman models with a non-zero cosmological constant. We shall restrict the discussion on the case of repulsive Λ-term, but the results can also be extended to the case of attractive Λ-term.

The geometry of a homogeneous and isotropic Friedman universe is given in the co-moving coordinates T, χ, θ, φ by

(80) $$ds^2 = -dT^2 + a^2(T)\left[d\chi^2 + \sum^2(\chi)(d\theta^2 + \sin^2\theta\, d\varphi^2)\right] ,$$

where

(81) $$\sum(\chi) = \sin\chi$$

for spatially closed universes; $k = +1$,

$$\sum(\chi) = \chi$$

for spatial flat universes; $k = 0$,

$$\sum(\chi) = \sinh\chi$$

for spatially hyperbolic universes; $k = -1$.

For dusty Friedman model the scale factor $a(T)$ is governed by

(82) $$(da/dT) = \tfrac{8}{3}\pi\varepsilon a^2 + \tfrac{1}{3}\Lambda a^2 - k ,$$

and by energy conservation law (recall that pressure is zero)

(83) $$\tfrac{8}{3}\pi\varepsilon a^3 = \text{const} = a_0 ;$$

see e.g. Misner et al. (1973). Thus we can find that the proper time of the cosmological-fluid particles is given by

(84) $$dT = \frac{\pm da}{\left[\tfrac{1}{3}\Lambda a^2 - k + a_0/a\right]^{1/2}} .$$

One can show that if $a_0 < \tfrac{2}{3}\Lambda^{-1/2}$ closed universes ($k = +1$) have two turning points of the expansion factor at

(85a) $$a_{t1} = 2\Lambda^{-1/2}\cos\left(\tfrac{1}{3}\pi + \tfrac{1}{3}\gamma\right) ,$$

(85b) $$a_{t2} = 2\Lambda^{-1/2}\cos\left(\tfrac{1}{3}\pi - \tfrac{1}{3}\gamma\right) ,$$

where

(86) $$\gamma = \arccos\tfrac{3}{2}a_0\Lambda^{1/2} ;$$

a_{t1} determines the maximal value of the expansion factor of the recollapsing universe, while a_{t2} gives the minimal value of the scale factor of the "turn around" universe without a big-bang singularity (see Misner et al., 1973). For $a_0 = \tfrac{3}{2}\Lambda^{1/2}$ we obtain the unstable static Einstein universe with

(87) $$a_s = \Lambda^{-1/2} .$$

If $a_0 > \tfrac{3}{2}\Lambda^{-1/2}$ the universe must expand forever from the big-bang singularity ($a = 0$).

On the other hand, Eq. (62), giving the proper time of particles moving along radial geodesics in the Schwarzschild-de Sitter spacetime can be rewritten in the form

(88) $$d\tau = \frac{\pm dr}{(2M/\tilde{R})^{1/2}\left[\tfrac{1}{6}\tilde{R}r^2/M - k + \tilde{R}/r\right]^{1/2}} ,$$

by defining

$$\Gamma = -k(2M/\tilde{R})\,. \tag{89}$$

If we now choose the hypersurface S_F to be the coordinate surface $\chi = \chi_b$ the spatial sections $T = $ = const of which are spheres with circumference

$$2\pi R_b = 2\pi\, a(T)\sum(\chi_b)\,, \tag{90}$$

then by comparing (84) and (88) we can see immediately that S_F and S_S can be identified if the matching condition

$$r_b = a(T)\sum(\chi_b) \tag{91}$$

is satisfied. Really, the circumferences $2\pi r_b$ and $2\pi R_b$ and proper times τ and T given by (88) and (84) are identified if (91) holds and the following conditions are satisfied:

$$\tilde{R} = a_0\sum(\chi_b)\,, \tag{92a}$$

$$\tilde{R}(\tfrac{1}{2}\tilde{R}/M)^{1/2} = a_0\,. \tag{92b}$$

Thus

$$\sum(\chi_b) = (2M/a_0)^{1/3}\,. \tag{93}$$

The cosmological matching problem in the case of a vanishing cosmological constant is discussed in Jantzen and Ruffini (1981). Note that our matching conditions (90)–(93) are the same as those obtained for $\Lambda = 0$; nevertheless there is one exception to this accordance. In the $\Lambda = 0$ case for closed universes it is $a_0 = a_m$, where a_m is the maximal value of the expansion factor; on the other hand in the $\Lambda \neq 0$ case we always have $a_0 \neq a_t$, but it is

$$r_{t1} = a_{t1}\sum(\chi_b)\,, \tag{94a}$$

$$r_{t2} = a_{t2}\sum(\chi_b)\,, \tag{94b}$$

$$r_s = a_s\sum(\chi_b)\,. \tag{94c}$$

In the case of the static Einstein universe the matching surface consists of particles in unstable equilibrium at r_s as given by (66). Finally it should be emphasized that in order to prove the possibility of constructing the Einstein-Strauss-de Sitter Universe, one must show that the extrinsic curvature of the matching surface has the same components in both the Schwarzschild-de Sitter interior and the Friedman exterior (see Misner et al., 1973).

Appendix A

The Latitudinal Motion of Particles with $E = 0$

As the parameters $\mathsf{K} = \mathscr{K}/(aE)^2$ and $b = \Phi/(aE)$ have been used in Sec. 3, the latitudinal motion in the case $E = 0$ must be considered separately. The turning points of the θ-motion are then given by the two-parameter family of curves

$$\mathscr{K}'_t(\theta;\tilde{\Phi}, y) = \frac{(1+y)^2\,\tilde{\Phi}^2}{\Delta_\theta \sin^2\theta} + \cos^2\theta\,, \tag{A1}$$

where

$$\mathscr{K}' = \frac{\mathscr{K}}{(am)^2}\,, \quad \tilde{\Phi} = \frac{\Phi}{am}\,; \quad (m \neq 0)\,.$$

If $\tilde{\Phi} \neq 0$ there is $\lim_{\theta\to 0}\mathscr{K}'_t = +\infty$ for $y > -1$, while $\lim_{\theta\to 0}\mathscr{K}'_t = \lim_{\theta\to\theta_{e-}}\mathscr{K}'_t = -\infty$, and $\lim_{\theta\to\theta_{e+}}\mathscr{K}'_t = $ $= +\infty$ for $y < -1$. The same limits hold for $\mathscr{K}'_t$ in the case of $m = 0$. The extreme points of the curves (A1) are located at $\theta = \frac{1}{2}\pi$ and along curves

$$\tilde{\Phi}_e^2 = -\frac{\Delta_\theta^2 \sin^4\theta}{(1+y)^2(1+y\cos 2\theta)}\,. \tag{A2}$$

Curves (A2) are defined (i.e. > 0) only for $|y| > 1$. Thus for $|y| < 1$ the curves $\mathscr{K}'_t$ have only minimum at $\theta = \frac{1}{2}\pi$. If $y > 1$, $\tilde{\Phi}_e^2$ is defined at $\theta \in (\theta_r, \frac{1}{2}\pi\rangle$, diverges at $\theta = \theta_r$ and has minimum $\tilde{\Phi}^2_{emin}$ at $\theta = \frac{1}{2}\pi$; therefore $\mathscr{K}'_t$ has a minimum at $\theta = \frac{1}{2}\pi$ for $\tilde{\Phi}^2 < \tilde{\Phi}^2_{emin}$ and a maximum for $\tilde{\Phi}^2 > \tilde{\Phi}^2_{emin}$.

If $y < -1$, $\tilde{\Phi}_e^2$ is defined at $\theta \in \langle 0, \theta_r)$; $\tilde{\Phi}_e^2$ is zero at $\theta = 0$ and diverges at $\theta = \theta_r$. As $\theta_r < \theta_e$, curves $\tilde{\Phi}_e^2$ determine the extrema of $\tilde{\mathscr{K}}_t$ in regions where $\Delta_\theta < 0$. In the case of $y < -1$ Eq. (20) must be used if $\Phi = 0$ $(E = 0)$:

$$\varrho^2\,\mathrm{d}\theta/\mathrm{d}\lambda = \pm[(\mathscr{K} - a^2m^2\cos^2\theta)\,\Delta_\theta]^{1/2}\,. \tag{A3}$$

Thus for $\mathscr{K} \neq -(am)^2/y$ particles must always have a turning point at θ_e, while if $\mathscr{K} = -(am)^2/y$, particles can approach θ_e only asymptotically as $W(\theta)$ has double zero at θ_e. Therefore, neither particles with $E = 0$ can cross the barrier at θ_e.

Appendix B

The Character of the Kerr-Newman-de Sitter Metric with $y < -1$

At $\theta > \theta_e$ the Kerr-Newman-de Sitter metric (2) has the quite usual form with signature $+2$, while at $\theta < \theta_e$ the signature of the metric is -2. Thus at the region $\theta < \theta_e$ for $\Delta_r > 0$ the third term, and for $\Delta_r < 0$ the first term, in the r.h.s. of (2) are timelike – this behaviour is inverse to that of the $\theta > \theta_e$-region.

Due to the normalization condition (7) eqs (10)–(17) determine the motion of tachyons in the $\theta < \theta_e$-region. Moreover, in the metric with signature -2 it is $p_\varphi = $ $= \partial\mathscr{L}/\partial(\mathrm{d}\varphi/\mathrm{d}\lambda) = -\Phi$, $p_t = \partial\mathscr{L}/\partial(\mathrm{d}t/\mathrm{d}\lambda) = E$, so that in Eqs (16), (17) the parameters E, Φ must be taken with opposite signs. Of course, these changes

of sings with respect to (8) and (9) have no influence on the discussion of the latitudinal motion in the Sec. 3., as we consider parameter $b = \Phi/aE$. On the other hand, the motion of test particles in the $\theta < \theta_e$-region will be governed by the same equations as the motion of tachyons in the $\theta > \theta_e$-region or in Kerr-Newman-de Sitter metrics with $y > -1$ (but, again, with opposite signs of E and Φ). One can immediately find that in the $\theta > \theta_e$-region tachyons with metamass $\tilde{m}$ will be moving along spacelike geodesics, which will be determined by eqs (10)–(13) with

$$(B1) \quad R(r) = P_r^2 - \Delta_r(\mathcal{K} - \tilde{m}^2 r^2),$$

$$(B2) \quad W(\theta) = (\mathcal{K} + a^2\tilde{m}^2 \cos^2\theta)\Delta_\theta - (P_\theta/\sin\theta)^2,$$

$$(B3) \quad \mathsf{P}_r = I[E(r^2 + a^2) - a\Phi],$$

$$(B4) \quad \mathsf{P}_\theta = I(aE \sin^2\theta - \Phi).$$

(Assuming that tachyons carry electric charge e, and their interaction with the black-hole background is given by Lagrangean (6), we find that (B3) = (16) and (B4) = (17).)

It is clear from eqs (15) and (B2) that no timelike, null or spacelike geodesic or test-particle trajectory can cross the surface of degeneracy $\theta = \theta_e$ as $\Delta_\theta = 0$ at θ_e, and $(\mathsf{P}_\upsilon/\sin\theta)^2$ enters the expression for $W(\theta)$ with negative sign. (Note that for the r-motion we have P_r^2 with positive sign in the expression for $R(r)$, and that is the reason why geodesics can cross the horizons where $\Delta_r = 0$.) In the special cases (see e.g. Appendix A) we have trajectories which approach the surface of degeneracy $\theta = \theta_e$ only asymptotically. Therefore we can conclude that regions $\theta < \theta_e$ and $\theta > \theta_e$ are geodesically disconnected by the surface $\theta = \theta_e$, and that these regions can be considered as separated spacetimes.

REFERENCES

Bičák, J.; Stuchlík, Z.: 1976, Bull. Astron. Inst. Czechosl. **27**, 129.

Carter, B.: 1973, in Black Holes (Eds C. DeWitt and B. S. DeWitt; Gordon and Breach, New York—London—Paris), p. 57.

Calvani, M.; Stuchlík, Z.: 1982, submitted to publ.

de Felice, F.; Calvani, M,: 1972, Nuovo Cim. **10B**, 447.

Gibbons, G. W.; Hawking, S. W.: 1977, Phys. Rev. **D 15**, 2738.

Gradstein, I. S.; Ryzhik, I. M.: 1971, Tablicy integralov, sum, ryadov i proizvedenij (Izd. Nauka, Moskva).

Hawking. S. W.; Ellis, G. F. R.: 1973, Large Scale Structure of Spacetime (Cambridge Univ. Press, New York).

Jantzen, R. T.; Ruffini, R.: 1981, University of Roma Preprint.

Lyubimov, V. A.; Novikov, E. G.; Nozik, V. Z.; Tretyakov, E. F.; Kosik, V. S.: 1980, Phys. Lett., **94B**, 266.

Misner, C. W.; Thorne, K. S.; Wheeler, J. A.: 1973, Gravitation (W. H. Freeman and Co., San Francisco).

Reines, F.; Sobel, H.; Pasierb, E.: 1980, Phys. Rev. Lett., **45** 1307.

Zel'dovich, J. B.; Syunyaev, R. A.: 1980, Pis'ma v Astron. Zh. **6**, 451.

THE DEPENDENCE OF THE SURFACE AND INTERIOR CHARACTERISCTICS OF THEORETICAL STELLAR MODELS, EVOLVED WITH VARIABLE G, ON THE AGE OF THE ISOCHRONE

A. D. Pinotsis and P. G. Laskarides

Department of Astronomy, University of Athens, Greece

Received 23 July 1981, revised 10 December 1981

ЗАВИСИМОСТЬ ПОВЕРХНОСТНЫХ И ВНУТРЕННИХ ХАРАКТЕРИСТИК ТЕОРЕТИЧЕСКИХ ЗВЕЗДНЫХ МОДЕЛЕЙ, РАССЧИТАННЫХ С ПЕРЕМЕННЫМ G, ОТ ВОЗРАСТА ИЗОХРОНЫ

Эволюция поверхностных и внутренних характеристик теоретических моделей звезд рассчитанных в предположении космологии Бранса-Дикке (уменьшение постоянной тятотения G во времени) обсуждается для моделей одинаковых масс на трех изохронах (возрастом в один, три и пять миллиардов лет). При увеличении возраста изохроны менее массивные модели ведут себя все-более и более как модели более массивные изохроны меньшего возраста, Теоретические изохроны не могут использоваться как индикаторы возраста, по крайней мере не так, как изохроны принятые с постоянным G, потому что положение и форма изохроны для скоплений равного возраста и химическоі о состава зависит также от начального значения G, равно как ог закона изменения G.

Bull. Astron. Inst. Czechosl. **34** (1983), 149—154.